Applied Radiation and Isotopes 69 (2011) 1830–1833

Contents lists available at ScienceDirect

Applied Radiation and Isotopes

journal homepage: www.elsevier.com/locate/apradiso

A phantom experiment for the evaluation of whole body exposure during BNCT using cyclotron-based epithermal neutron source (C-BENS)

T. Tsukamoto [a,*], H. Tanaka [b], H. Yoshinaga [b], T. Mitsumoto [c], A. Maruhashi [b], K. Ono [b], Y. Sakurai [b]

[a] Graduate School of Engineering, Kyoto University, Yoshida Honmachi, Sakyo-ku, Kyoto 606-8501, Japan
[b] Research Reactor Institute, Kyoto University, Asashiro-nishi 2-1010, Kumatori-cho, Osaka 590-0494, Japan
[c] Sumitomo Heavy Industries, Ltd., Osaki 2-1-1, Shinagawa, Tokyo 141-6025, Japan

ARTICLE INFO

Available online 21 March 2011

Keywords:
Cyclotron-based epithermal neutron source
Whole body exposure
Water phantom
Dose equivalent

ABSTRACT

At Kyoto University Research Reactor Institute (KURRI), cyclotron-based epithermal neutron source was installed in December 2008, and the supplementary construction works have been performed. As of December 2010, the various irradiation characteristics important for BNCT were mostly evaluated. The whole body exposure during BNCT medical irradiation is one of the important characteristics.

In this article, measurements of absorbed dose for thermal and fast neutrons and gamma-ray at ten positions corresponding to important organs are reported.

1. Introduction

At KURRI, cyclotron-based epithermal neutron source (C-BENS) was installed in December 2008, and neutron generation test was begun in March 2009. C-BENS consists of a cyclotron accelerator that can produce 1 mA, 30 MeV protons, a beam transport system with a neutron production beryllium target and the moderator for reducing the neutron energy from high energy up to 28 MeV to epithermal energy (Tanaka et al., 2009a). As of December 2010, the various irradiation characteristics important for BNCT, physical characteristics test and biological characteristics test using cell and mice were mostly evaluated. It was confirmed that the epithermal neutron beam intensity is about twice larger than that of heavy water neutron irradiation facility (HWNIF) of Kyoto University Reactor (KUR) (Sakurai and Kobayashi , 2002). However, fast neutron energy generated by beryllium target of C-BENS was higher than that of HWNIF. Hence, it is necessary to evaluate the whole body exposure caused by fast neutrons during medical BNCT irradiation.

To experimentally evaluate absorbed dose in whole human body, a water-filled phantom modified for whole human body was prepared. The measurements of thermal and fast neutron flux using neutron activation foils, and gamma-ray dose using thermo-luminescent dosimeters (TLDs) were performed. In this article, the evaluations of absorbed dose based on the measurement results at the locations of important organs are reported.

2. Material and methods

2.1. A human whole-body phantom

The human whole-body phantom is 170 cm in height, and consists of some rectangular acrylic-resin cases filled with water as shown in Fig. 1.

Thermal neutron flux was measured with neutron activation foil method using bare gold foils and cadmium-covered gold foils. The gold foils are 10 mm in diameter with the thickness of 0.05 mm. The fast neutron flux over the energy of 0.5 MeV was determined with the activity of indium foils. The indium foils are 20 mm in diameter with the thickness of 0.10 mm. Gamma-ray dose was measured by using TLDs. TLDs were made of beryllium oxide sealing in quartz cell in order to reduce the sensitivity for neutrons. The gold foils and TLDs were placed at ten positions: (1) brain, (2) thyroid, (3) esophagus, (4) bone marrow, (5) lung, (6) stomach, (7) liver, (8) colon, (9) bladder and (10) gonad. And the indium foils were positioned at nine positions except for the brain.

For the irradiation tests, it was assumed that a target volume was positioned at the depth of 2 cm from the left lateral surface of the head phantom and irradiated in the supine position. The phantom was attached to the beam aperture and the schematic layout of this experiment is shown in Fig. 2. The shape of the beam is circular and the size of irradiation field is 10 cm in diameter. After the irradiation, the activities of the gold and indium foils were measured with high-purity germanium detector (model GEM20P4, ORTEC).

2.2. Evaluation of the absorbed dose

In order to calculate the absorbed dose at ten positions, the neutron and gamma-ray sources at the surface of collimator,

* Corresponding author. Tel./fax: +81 72 451 2604.
E-mail addresses: t.tsukamoto@ft5.ecs.kyoto-u.ac.jp, tsukamoto3251@gmail.com (T. Tsukamoto).

0969-8043/$ - see front matter © 2011 Elsevier Ltd. All rights reserved.
doi:10.1016/j.apradiso.2011.03.013

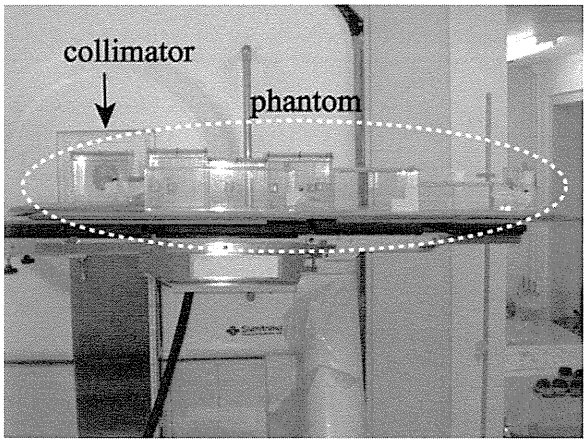

Fig. 1. Photograph of the experiments using a human whole-body phantom.

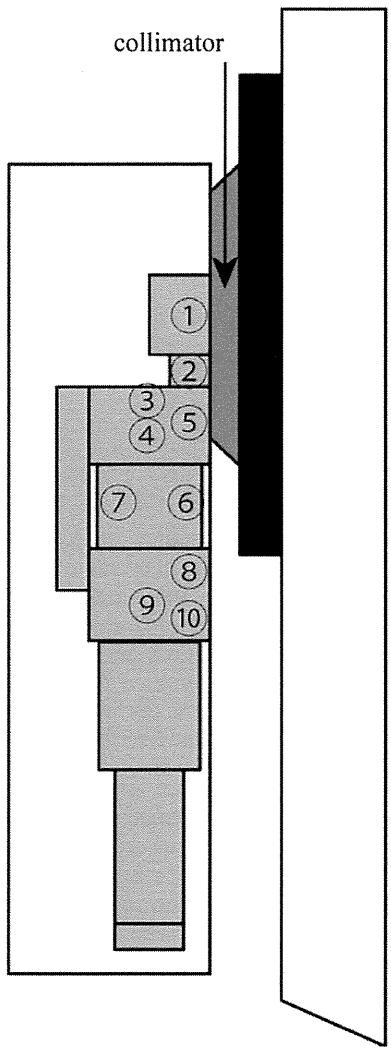

Fig. 2. Schematic layout of the irradiation tests in the supine position using a whole-body phantom. The numbers represent the assumed important organs 1, head; 2, thyroid; 3, esophagus; 4, bone marrow; 5, lung; 6, stomach; 7, liver; 8, colon; 9, bladder; and 10, gonad.

which were estimated by previous work (Tanaka et al., 2009a), were used. In the calculation, the collimator structures were modeled and the sources were modeled up to 150 cm in radius. The typical neutron spectra near the organs such as head, lung

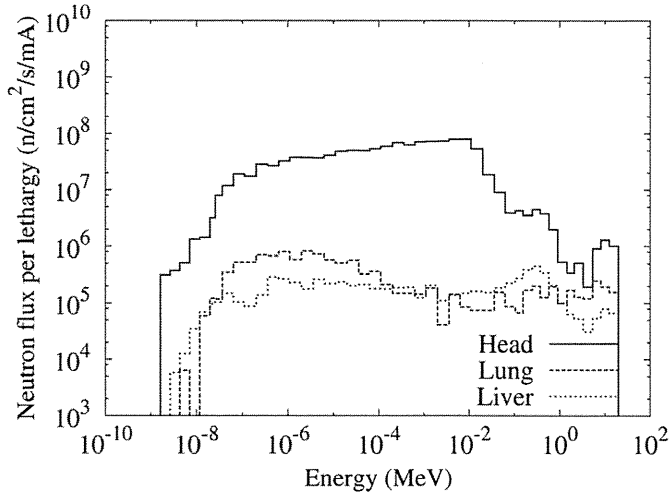

Fig. 3. Typical neutron energy spectra on the surface of head, and near lung and liver.

and liver are shown in Fig. 3. The calculated thermal and fast neutron absorbed doses were derived from the multiplication between the neutron spectrum calculated by MCNPX and kerma factors (Chadwick et al., 1999) considering the elemental components of each organ (ICRU, 1992).

2.2.1. Absorbed dose for thermal neutrons

The calculated data of absorbed dose for thermal neutrons at each organ is normalized with the ratio of the measured and calculated data at the peak of the thermal neutron flux distribution in the head phantom. In this experiment, the activity at the peak of the thermal neutron distribution is highest compared with other position. Therefore, it is easy to obtain less statistical error. We select the location at the peak position to normalize.

On the other hand, to estimate the measured absorbed dose due to thermal neutrons, the calculated absorbed dose data was multiplied with the measured-to-calculated thermal neutron flux ratio.

2.2.2. Absorbed dose for fast neutrons

The calculated fast neutron absorbed dose at each organ is normalized with the ratio of the measured-to-calculated indium reaction rate at the position of thyroid in the neck phantom. In this experiment, the activity at the thyroid is highest compared with other position. Therefore, it is easy to obtain less statistical error. We select the location at the position of thyroid to normalize. The calculated reaction rate was derived from the multiplication of the energy spectrum and the cross-section data of JENDL/D-99.

On the other hand, to estimate the measured fast neutron absorbed dose, the calculated absorbed dose data was multiplied with the measured-to-calculated indium reaction rate ratio.

2.2.3. Gamma-ray dose

In order to estimate primary gamma-rays generated from the C-BENS components and secondary gamma-rays caused by the reactions between the neutrons and human body elements such as hydrogen, the calculations using F4 tally of MCNPX code without electron transport were performed separately with the neutron and gamma-ray sources. To derive the gamma ray dose, the flux to dose conversion factor was used. The measured primary and secondary gamma-ray doses are estimated by using the primary-to-secondary gamma-ray dose ratio calculated with

MCNPX. To estimate the calculated gamma-ray absorbed dose, data was normalized with the ratio of the measured and calculated data at the position of thyroid in the neck phantom.

3. Results and discussion

From the phantom experiments, it was confirmed that the peak of the thermal neutron flux distribution was at 2 cm depth from the left lateral surface in the head phantom, and the peak value for brain was almost 1.0×10^9 cm^{-2} s^{-1} per proton beam current of 1 mA. The thermal neutron flux of thyroid was 2.8×10^7 cm^{-2} s^{-1} per proton beam current of 1 mA and was much larger than that of the other organs. Because the thyroid was located near the target volume, the influence due to the thermal neutrons produced in brain was larger. In terms of the fast neutrons, ^{115}In(n,n′)^{115m}In reaction rate, the value of thyroid was 1.2×10^{-19} s^{-1} atom^{-1} per proton beam current of 1 mA and was more than twice larger than that of other organs. Fig. 4 shows the calculated neutron energy spectrum of lung which is one of the sensitive organs.

The gamma-ray absorbed dose in brain reached the maximum value at 2.7 cm depth from the left lateral surface. The absorbed dose for thyroid was about twice the values for the other organs.

Table 1 shows the calculated-to-measured absorbed dose ratios for thermal and fast neutrons and gamma-ray at the each organ. As a result, the measured thermal and fast neutron absorbed doses were in agreement with the calculated data within the factor of 0.4–2. The discrepancy between the calculated and measured data might be caused by the difference of angular distribution between calculation and experiment.

The estimated uncertainties of the measured thermal and fast neutron flux were 5% and 10%, respectively. The estimated uncertainties of the calculated thermal and fast neutron flux were less than 1%. The measured gamma-ray dose was in good agreement with the calculated data. The estimated uncertainties of the measured and calculated gamma-ray dose were 10% and 1%, respectively. Therefore, it is confirmed that the calculation for gamma-ray can simulate the measurements except in lung. The discrepancy between the calculated and measured gamma-ray doses for lung might be caused by the difference of experimental location of TLD compared with calculation location.

To evaluate the whole body exposure during BNCT medical irradiation, absorbed doses for thermal and fast neutrons were converted to relative biological effectiveness (RBE)-weighted dose. Fig. 5 shows the RBE-weighted dose for each organ. The

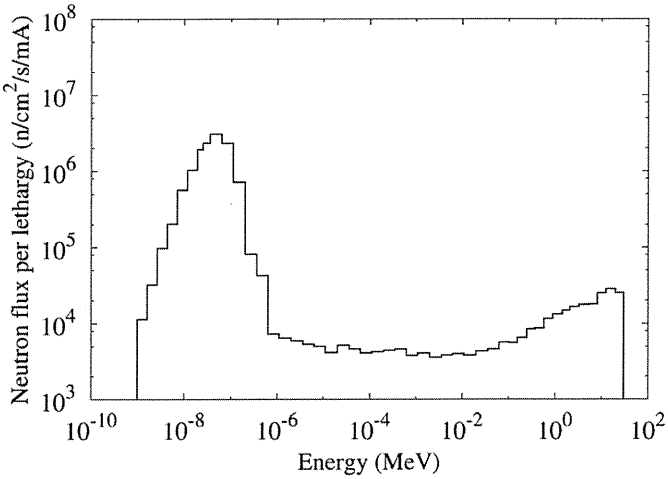

Fig. 4. Calculated neutron energy spectrum at the position of lung.

Table 1
Calculated-to-measured dose ratios for the thermal and fast neutrons and gamma-ray.

Organ	Ratio		
	Thermal neutron	Fast neutron	Gamma-ray
Thyroid	1.72	1.00	1.00
Esophagus	0.66	1.88	0.95
Bone marrow	0.59	1.34	0.96
Lung	1.11	0.89	1.52
Stomach	0.65	1.13	1.00
Liver	0.46	1.21	1.03
Colon	0.52	0.92	1.01
Bladder	0.43	0.86	0.93
Gonad	0.36	0.66	1.06

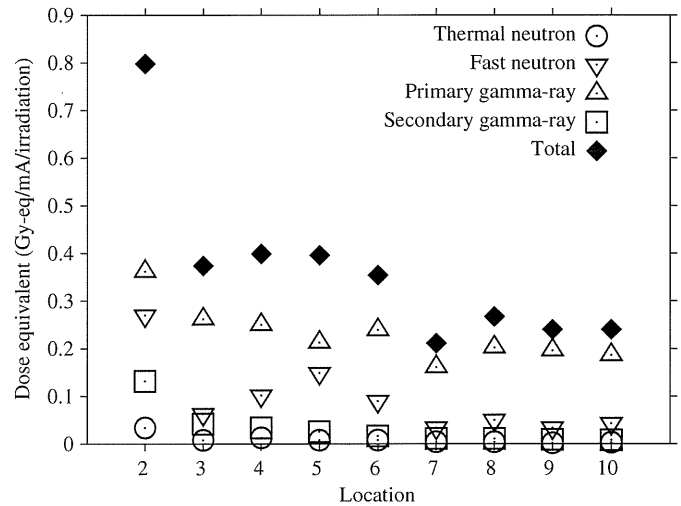

Fig. 5. RBE-weighted doses at locations of 2, thyroid; 3, esophagus; 4, bone marrow; 5, lung; 6, stomach; 7, liver; 8, colon; 9, bladder; and 10, gonad.

irradiation time was assumed 40 min considering typical irradiation. Both of RBEs for thermal and fast neutrons are 3.0, respectively (Tanaka et al., 2009b). It was found that the gamma-ray dose was larger than the other dose components. At the position of thyroid, primary gamma-ray dose accounted for 45% of total dose and fast neutron dose accounted for 34%. And secondary gamma-ray dose accounted for 17% of total dose, because thyroid was located near the target volume with the distance of 13 cm, and thermal neutrons generated at the target was reduced during reaching into thyroid.

On the other hand, at other positions, the total dose of primary gamma-ray and fast neutron accounted for a large fraction of total dose. Hence it is guessed that the whole body exposure can be reduced by shielding the primary gamma-rays generated from the C-BENS components and fast neutrons.

4. Conclusions

The whole body exposure was experimentally evaluated using the activation foils for thermal and fast neutrons and TLDs for gamma-rays. It is confirmed that the calculated MCNPX simulation results for whole body exposure were in agreement with the measured data within the factor of 0.4–2. It was also found that the primary gamma-ray dose and fast neutron dose were main components of the whole body exposure. Based on this research, the additional shields, polyethylene containing LiF and lead plate, were already set outside the aperture in the gap between a

patient and C-BENS to reduce primary gamma-ray and fast neutron dose. The shielding also has halved the thermal neutron fluence and dose.

References

Chadwick, M., Barschall, H., Caswell, R., DeLuca, P., Hale, G., Jones, D., MacFarlane, R., Meulders, J., Schuhmacher, H., Schrewe, U., Wambersie, A., Young, P., 1999. A consistent set of neutron kerma coefficients from thermal to 150 MeV for biologically important materials. Med. Phys. 26 (6), 974–991.

ICRU, 1992. Photon, electron, proton, and neutron interaction data for body tissues, ICRU Report 46, Bethesda, MD.

Sakurai, Y., Kobayashi, T., 2002. The medical-irradiation characteristics for neutron capture therapy at the heavy water neutron irradiation facility of Kyoto University Research Reactor. Med. Phys. 29 (10), 2328–2337.

Tanaka, H., Sakurai, Y., Suzuki, M., Masunaga, S., Kinashi, Y., Kashino, G., Liu, Y., Mitsumoto, T., Yajima, S., Tsutsui, H., Maruhashi, A., Ono, K., 2009a. Characteristics comparison between a cyclotron-based neutron source and KUR-HWNIF for boron neutron capture therapy. Nucl. Instrum. Methods B 267, 1970–1977.

Tanaka, H., Sakurai, Y., Suzuki, M., Takata, T., Masunaga, S., Kinashi, Y., Kashino, G., Liu, Y., Mitsumoto, T., Yajima, S., Tsutsui, H., Takada, M., Maruhashi, A., Ono, K., 2009b. Improvement of dose distribution in phantom by using epithermal neutron source based on the Be(p,n) reaction using a 30 MeV proton cyclotron accelerator. Appl. Radiat. Isot. 67, S258–S261 (13th International congress on neutron capture therapy BNCT: a new option against cancer).

Deficit of tRNA^{Lys} modification by Cdkal1 causes the development of type 2 diabetes in mice

Fan-Yan Wei,[1] Takeo Suzuki,[2] Sayaka Watanabe,[1] Satoshi Kimura,[2] Taku Kaitsuka,[1] Atsushi Fujimura,[3] Hideki Matsui,[3] Mohamed Atta,[4] Hiroyuki Michiue,[3] Marc Fontecave,[4] Kazuya Yamagata,[5] Tsutomu Suzuki,[2] and Kazuhito Tomizawa[1]

[1]Department of Molecular Physiology, Faculty of Life Sciences, Kumamoto University, Kumamoto, Japan. [2]Department of Chemistry and Biotechnology, School of Engineering, The University of Tokyo, Tokyo, Japan. [3]Department of Physiology, Okayama University Graduate School of Medicine, Dentistry and Pharmaceutical Sciences, Okayama, Japan. [4]Institut de Recherches en Technologie et Sciences pour le Vivant IRTSV-LCBM, UMR 5249, CEA/CNRS/UJF, CEA-Grenoble, Grenoble, France. [5]Department of Medical Biochemistry, Faculty of Life Sciences, Kumamoto University, Kumamoto, Japan.

The worldwide prevalence of type 2 diabetes (T2D), which is caused by a combination of environmental and genetic factors, is increasing. With regard to genetic factors, variations in the gene encoding Cdk5 regulatory associated protein 1–like 1 (Cdkal1) have been associated with an impaired insulin response and increased risk of T2D across different ethnic populations, but the molecular function of this protein has not been characterized. Here, we show that Cdkal1 is a mammalian methylthiotransferase that biosynthesizes 2-methylthio-N^6-threonylcarbamoyladenosine (ms^2t^6A) in tRNA^{Lys}(UUU) and that it is required for the accurate translation of AAA and AAG codons. Mice with pancreatic β cell–specific KO of Cdkal1 (referred to herein as β cell KO mice) showed pancreatic islet hypertrophy, a decrease in insulin secretion, and impaired blood glucose control. In Cdkal1-deficient β cells, misreading of Lys codon in proinsulin occurred, resulting in a reduction of glucose-stimulated proinsulin synthesis. Moreover, expression of ER stress–related genes was upregulated in these cells, and abnormally structured ER was observed. Further, the β cell KO mice were hypersensitive to high fat diet–induced ER stress. These findings suggest that glucose-stimulated translation of proinsulin may require fully modified tRNA^{Lys}(UUU), which could potentially explain the molecular pathogenesis of T2D in patients carrying *cdkal1* risk alleles.

Introduction

Type 2 diabetes (T2D) is caused by a combination of genetic and environmental factors. Recent advances in whole-genome association studies have identified a number of genetic variations associated with T2D (1–4). The Cdk5 regulatory associated protein 1–like 1 (*cdkal1*) gene is one of the most reproducible risk genes in T2D across different ethnic populations (5). Variations in *cdkal1* have been associated with impaired insulin secretion and increased risk of T2D (6–8). Although there is increasing evidence associating single nucleotide polymorphisms in *cdkal1* with T2D, the molecular function of Cdkal1 is unknown.

We recently identified Cdkal1 as a member of the methylthiotransferase (MTTase) family, a subfamily of the radical S-adenosylmethionine (SAM) superfamily (9). The MTTase family utilizes SAM and [4Fe-4S] clusters to catalyze the methylthiolation of various substrates. For instance, MiaB, a bacterial MTTase protein, catalyzes the methylthiolation of N^6-isopentenyladenosine (i^6A) to generate 2-methylthio-N^6-isopentenyladenosine (ms^2i^6A) at position 37 (A^{37}), 3′ adjacent to the anticodon in some tRNAs (10, 11). This hypermodification of A^{37} is essential for the efficient and accurate translation of cognate codons by the ribosome (12, 13). We have shown that Cdkal1 (and its bacterial homolog YqeV) catalyze the methylthiolation of N^6-threonyl carbamoyl adenosine (t^6A) to synthesize 2-methylthio-N^6-threonyl carbamoyl adenosine (ms^2t^6A) for tRNA in bacteria (9). However, the enzymatic characteristics of Cdkal1 in mammalian cells and its relevance to T2D are completely unknown. By using pancreatic β cell–specific Cdkal1 KO mice (referred to herein as β cell KO mice), we show that Cdkal1 has critical roles in the quality control of protein translation and is relevant to T2D.

Results

Cdkal1 catalyzes ms^2t^6A modification of mammalian tRNA^{Lys}(UUU). To determine the biochemical function of Cdkal1 in mammalian cells and its relevance to T2D, we used mass spectrometric analysis to examine modified bases in total RNA from MIN6 cells, a pancreatic β cell–derived insulinoma cell line, and HeLa cells, a human-derived cell line (Figure 1B). As expected, the proton adduct ms^2t^6A (m/z 459) could be clearly detected along with t^6A (m/z 413) in both cell types (Figure 1B). In addition, we also detected ms^2t^6A in total RNA from various mouse tissues (Supplemental Figure 1; supplemental material available online with this article; doi:10.1172/JCI58056DS1). To investigate whether Cdkal1 was involved in the ms^2t^6A modification, we examined total RNA isolated from the pancreas of WT and *Cdkal1*$^{-/-}$ mice. The ms^2t^6A modification was detected only in the WT mice but not in the *Cdkal1*$^{-/-}$ mice (Figure 1C). These results suggest that Cdkal1 only catalyzes the ms^2t^6A modification in mammalian cells. Because ms^2t^6A is present at position 37 of tRNA^{Lys} in *Bacillus subtilis* (14, 15), we isolated 2 species of tRNA^{Lys} (tRNA^{Lys}[UUU] [Figure 1A] and tRNA^{Lys}[CUU] [Supplemental Figure 2A]) from mouse livers and performed an RNA

Authorship note: Takeo Suzuki and Sayaka Watanabe contributed equally to this work.

Conflict of interest: The authors have declared that no conflict of interest exists.

Citation for this article: *J Clin Invest.* 2011;121(9):3598–3608. doi:10.1172/JCI58056.

fragment analysis. ms^2t^6A was specifically found at position 37 of $tRNA^{Lys}$(UUU) in WT liver (Figure 1D), whereas $tRNA^{Lys}$(CUU) bore t^6A at position 37 (Supplemental Figure 2B). As no fragment containing t^6A was detected in $tRNA^{Lys}$(UUU) of WT liver, the methylthio modification appeared to be introduced universally (Figure 1D). When the nucleosides from the flow-through fraction after the isolation of $tRNA^{Lys}$(UUU) were analyzed, no ms^2t^6A could be detected (Supplemental Figure 3), suggesting that ms^2t^6A is a modification specific to $tRNA^{Lys}$(UUU). In contrast, the ms^2t^6A-containing fragment (m/z 1172.16) was completely replaced with a t^6A-containing fragment (m/z 1126.17) in $tRNA^{Lys}$(UUU) isolated from livers of *Cdkal1*$^{-/-}$ mice (Figure 1D). These results demonstrate that mouse Cdkal1 is a methylthiolase that converts t^6A to ms^2t^6A in $tRNA^{Lys}$(UUU).

The ms^2t^6A modification is required for decoding fidelity. The 2-methylthio modification ms^2i^6A is important for preventing the misreading and frame-shifting of cognate codons during protein translation in bacteria (12–14). These observations prompted us to speculate that the 2-methylthio modification ms^2t^6A in $tRNA^{Lys}$(UUU) is also required for translational accuracy. To examine whether the ms^2t^6A modification prevents either the frame-shifting or misreading of $tRNA^{Lys}$(UUU)'s cognate codons (AAA and AAG), we utilized a dual luciferase-based reporter assay in WT *B. subtilis* and *yqeV*-deficient *B. subtilis* (Δ*yqeV*), which lacks the ms^2t^6A modification (Supplemental Figure 4A, Figure 1E, and ref. 16). Because Lys529 in *firefly* luciferase is essential for enzymatic activity, the misreading or frameshifting of this codon would result in a loss of *firefly* luciferase activity (17, 18). Two constructs in which Lys529 is encoded by AAA or AAG codons were introduced into WT and Δ*yqeV* strains, and relative *firefly* luciferase activity was measured (Figure 1E). In the Δ*yqeV* strain under noninducible conditions (–IPTG), a specific reduction in *firefly* luciferase activity was observed with the AAA construct, but not with the AAG construct (Figure 1E). Under inducible conditions (+IPTG), a marked reduction in *firefly* luciferase activity was observed with both constructs in the Δ*yqeV* strain, and an even greater reduction in activity was observed with the AAG construct (Figure 1E), although the IPTG-induced protein level of the *renilla-firefly* fusion protein was the same in the WT and Δ*yqeV* strains (Figure 1F). We next determined whether the 2-methylthio modification ms^2t^6A is involved in the reading frame maintenance of the relevant codons. We employed constructs that fused *Renilla* and *firefly* luciferases separated by a short sequence containing a +1 frameshift site (Supplemental Figure 4B). We observed no significant frameshift activity of either construct in the Δ*yqeV* strain as compared with the WT strain. These results suggest that the 2-methylthio modification ms^2t^6A in $tRNA^{Lys}$(UUU) is important for preventing the misreading of its cognate codons, especially when the rate of translation is relatively high.

Cdkal1 is an ER-localizing protein that is functionally dissociated with Cdk5/p35. Cdkal1 was ubiquitously expressed in mouse tissues through all the developmental stages and was especially abundant in the heart, kidney, and pancreas (Supplemental Figure 5). To investigate the subcellular distribution of Cdkal1, HEK293 and MIN6 cells were transfected with EGFP-Cdkal1 and ER-tracker. EGFP-Cdkal1 colocalized with ER-tracker (Figure 2A). Moreover, Cdkal1 was also colocalized with endogenous Bip, an ER protein (Figure 2B). Cdkal1 has 3 unique domains, a radical SAM domain, a TRAM domain, and a hydrophobic domain (Figure 2C). Both the radical SAM domain (a catalytic domain) and the TRAM domain (a potential tRNA-binding domain) are conserved among mammals and bacteria (9). In contrast, the hydrophobic domain at the C terminus exists only in mammalian Cdkal1 (9). This hydrophobic domain was determined to carry the ER-localization signal because deletion of this domain disrupted ER localization (Figure 2D). Furthermore, endogenous Cdkal1 was detected in the rough ER fraction purified from mouse liver (Supplemental Figure 6). The ER localization was finally confirmed by immunoelectron microscopic examination in EGFP-Cdkal1–transfected MIN6 cells (Figure 2E).

We previously reported that Cdk5 regulates insulin secretion in pancreatic β cells (19). Cdkal1 may function through interaction with a Cdk5 regulatory subunit, p35, as Cdk5rap1, an amino acid homolog of Cdkal1, interacts with p35 and inhibits Cdk5 activity (20, 21). However, Cdkal1 neither interacted with p35 in HEK293 cells overexpressing p35 nor inhibited Cdk5 activity in vitro (Supplemental Figure 7), suggesting that the molecular function of Cdkal1 in β cells is independent of the pathway in which Cdk5/p35 participates.

Cdkal1 deficiency in β cells causes glucose intolerance. To investigate the physiological functions of Cdkal1 in pancreatic β cells, β cell–specific Cdkal1-deficient mice (β cell KO) were generated by crossing transgenic mice in which exon 5 of *cdkal1* was floxed by the LoxP sequence with transgenic mice in which Cre recombinase was regulated under the control of the rat insulin promoter (Supplemental Figure 8A). Exon 5 of *cdkal1* was deleted in the pancreatic islets of β cell KO mice, but not the other tissues of the β cell KO mice, (Supplemental Figure 8B). Cdkal1 protein expression was faint in the islets of β cell KO mice compared with that in the islets of littermate control mice (Flox) (Figure 3A). In contrast, the same level of Cdkal1 was observed in kidney of Flox mice and β cell KO mice (Figure 3A). The β cell KO mice showed normal development (Figure 3B). Immunohistochemical analyses revealed no obvious morphological abnormalities in α or β cells in the pancreatic islets of β cell KO mice relative to Flox mice (Figure 3C). However, we noticed that KO islets were larger than Flox islets, and we performed a detailed analysis to investigate islet area. We divided the islets into 3 groups: small islets (0–5,000 μm^2), medium islets (5,001–10,000 μm^2), and large islets (>10,000 μm^2), and we calculated the relative abundance of each group. In β cell KO mice, the number of small islets was significantly lower than in Flox mice, and the number of large islets was significantly greater (Figure 3D). Because there was no difference in total islet number between β cell KO and Flox mice (data not shown), pancreatic islets in β cell KO mice may be able to lapse into a hypertrophic condition.

Because insulin secretion is impaired in patients with variants of the *cdkal1* gene (6–8), the mice were given an intraperitoneal glucose tolerance test (IPGTT). The β cell KO mice showed glucose intolerance compared with the Flox mice at 5 and 10 weeks after birth (Figure 3E). Moreover, plasma insulin levels 15 minutes after the glucose challenge were significantly lower in the β cell KO mice (Figure 3F). We also investigated insulin secretion in islets isolated from Flox and β cell KO mice. After 16.7 mM glucose stimulation, the insulin level was significantly lower in β cell KO mice than in Flox mice (Figure 3G). Because patients with variants of the *cdkal1* gene showed a specific impairment of first-phase insulin secretion (6), we investigated whether a deficiency of Cdkal1 has any effect on the biphasic secretion of insulin. We examined glucose-stimulated insulin secretion in perifused islets isolated from Flox and β cell KO mice. The KO islets showed impaired first-phase, but not second-phase, insulin secretion upon stimulation with 16.7 mM glucose compared with the Flox islets (Figure 3H). Furthermore, we also

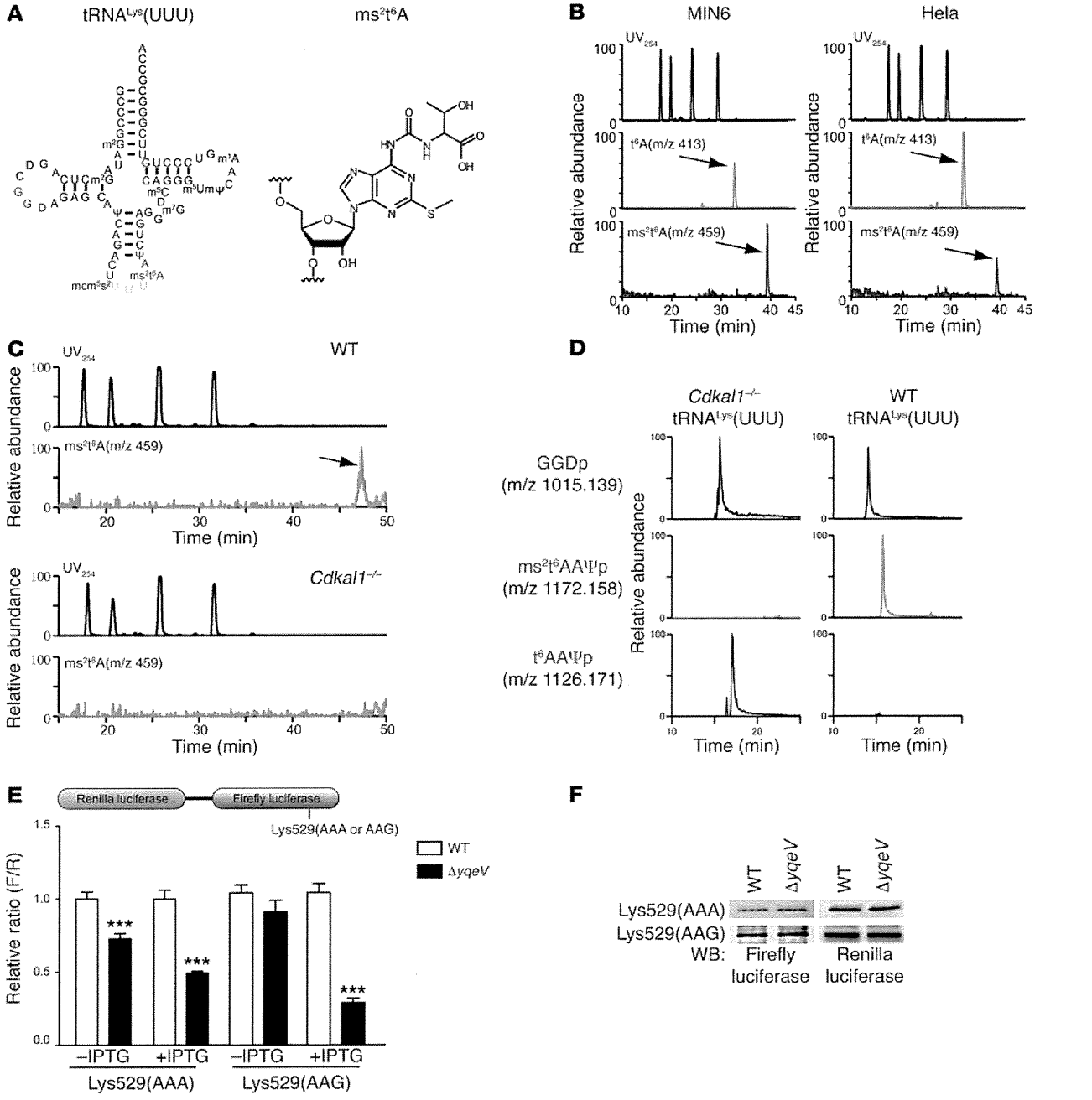

Figure 1

Methylthiolation of tRNA^{Lys}(UUU) by Cdkal1 controls the decoding accuracy of the lysine codon. (**A**) The molecular structure of tRNA^{Lys}(UUU) and ms^{2}t^{6}A. (**B**) Results of a mass spectrometric analysis of the ms^{2}t^{6}A modification of tRNA in MIN6 and HeLa cells. The upper panels show the UV trace, and the middle and lower panels show the mass chromatograms for detecting t^{6}A (m/z 413, arrow) and ms^{2}t^{6}A (m/z 459, arrow), respectively. (**C**) Results of a mass spectrometric analysis of the ms^{2}t^{6}A modification of tRNA isolated from the pancreas of *Cdkal1*$^{-/-}$ and WT mice. The arrow indicates ms^{2}t^{6}A (m/z 459). (**D**) Modification of tRNA^{Lys}(UUU) isolated from the liver of *Cdkal1*$^{-/-}$ and WT mice. The upper panels show mass chromatograms of GGDp fragments in tRNA^{Lys}(UUU). The middle and lower panels show mass chromatograms of ms2t6AAΨp fragments and t6AAΨp fragments, respectively. (**E**) WT and Δ*yqe*V cells were transformed with a reporter plasmid in which both Renilla renilla and firefly luciferases are cloned with the lac promoter (upper panel). Relative activity was determined by normalizing firefly luciferase intensity to renilla luciferase intensity (F/R, lower panel). Data are presented as the mean ± SEM, and asterisks indicate statistical significance determined by Student's *t* test. ***$P < 0.001$; $n = 4$. (**F**) The expression level of the fusion protein of firefly and renilla luciferase after IPTG treatment induction was determined in WT and Δ*yqe*V cells (**E**) by Western blot.

investigated insulin secretion in Flox and β cell KO mice under normal feeding conditions. The mice were fasted overnight and then re-fed for 1.5 hours. Plasma insulin levels in the fasting condition and postprandial condition were determined (Figure 3I). There was a significant decrease in postprandial insulin secretion in β cell KO mice when compared with Flox mice. These results suggest that Cdkal1 deficiency in pancreatic β cells impairs glucose-stimulated insulin secretion and thus induces glucose intolerance.

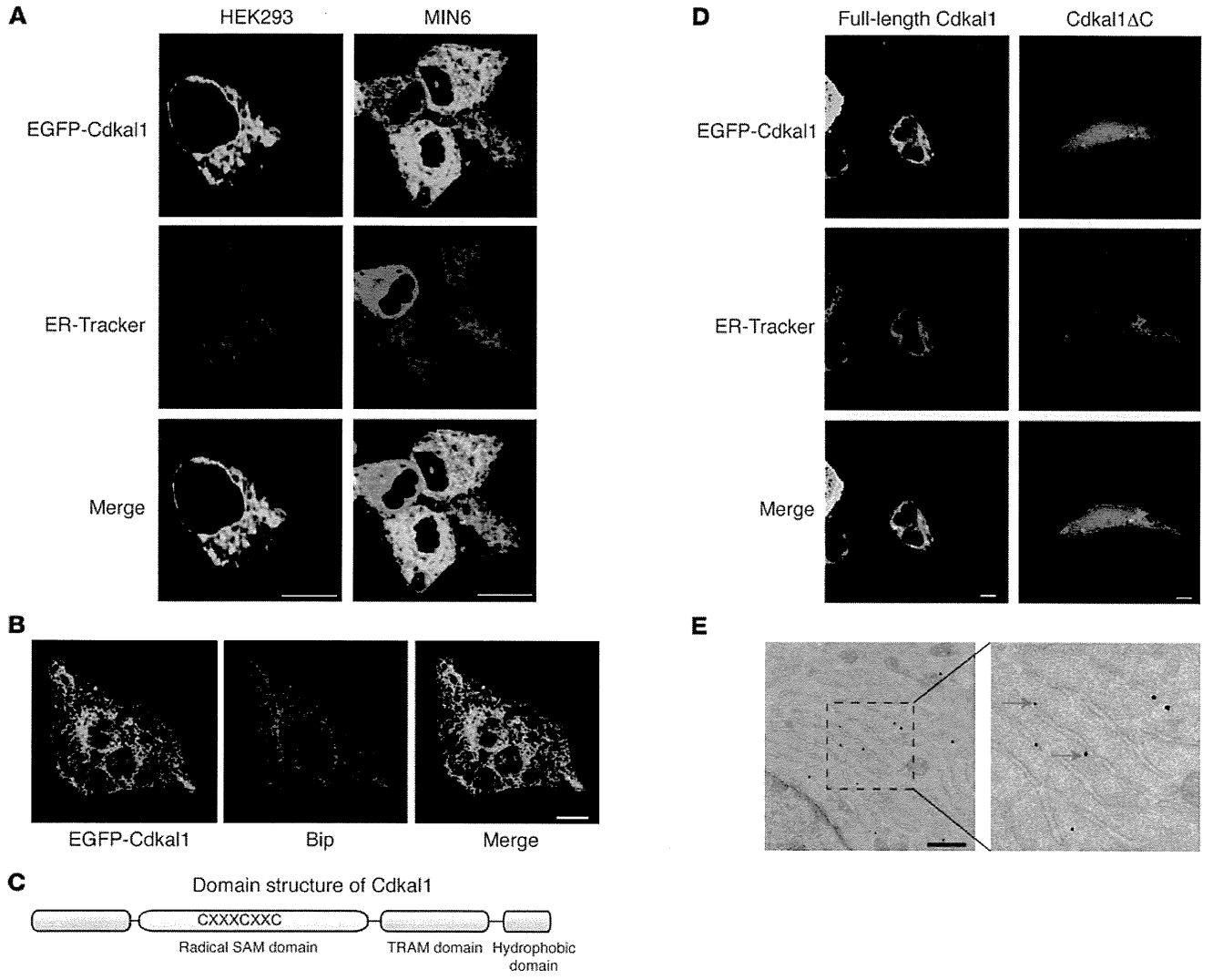

Figure 2

Cdkal1 localizes on ER through its hydrophobic domain. (**A**) Colocalization of overexpressed Cdkal1-EGFP (green) and ER-tracker (red) on ER in HEK293 cells and MIN6 cell. Scale bars: 10 μm. (**B**) Colocalization of overexpressed Cdkal1-EGFP (green) with endogenous Bip in HEK293 cells. Scale bar: 10 μm. (**C**) The domain structure of Cdkal1 protein. (**D**) EGFP-tagged full-length Cdkal1 or Cdkal1 with truncation of C terminus hydrophobic domain (Cdkal1ΔC) was transfected in HeLa cells together with ER-tracker. Localization of full-length Cdkal1 or Cdkal1ΔC was visualized using confocal microscope. Scale bars: 10 μm. (**E**) MIN6 cells were transfected with Cdkal1-EGFP, and the localization of Cdkal1 was determined by immunoelectronic microscopic examination. Arrows indicate EGFP-Cdkal1 signal on ER. Scale bar: 0.5 μm.

Cdkal1 deficiency induces aberrant proinsulin synthesis. Given the molecular function of Cdkal1 in *B. subtilis* (Figure 1), we speculated that Cdkal1 deficiency in pancreatic β cells decreases the decoding fidelity in lysine codon due to insufficient modification in $tRNA^{Lys}(UUU)$. The Lys residue is particularly important for processing proinsulin to generate mature insulin and C-peptide because 1 of the 2 Lys residues in human proinsulin is located at the cleavage site between the C-peptide and A chain of insulin. Thus, misreading of Lys codon in proinsulin by insufficiently modified $tRNA^{Lys}(UUU)$ might result in aberrant processing of (pro)insulin and subsequent glucose intolerance. To investigate misreading of Lys codon in Cdkal1-deficient β cells, pancreatic islets isolated from both β cell KO and Flox mice were labeled with both ^{14}C-lysine and ^{3}H-leucine. If misreading of Lys codon occurs in Cdkal1-deficient β cells, we would observe a change in the ratio of incorporation of ^{14}C-lysine to ^{3}H-leucine in (pro)insulin when compared with the incorporation ratio in Flox β cells. As expected, there was a significant decrease of relative incorporation of ^{14}C-lysine in (pro)insulin in Cdkal1-deficient β cells when compared with Flox β cells (KO: 0.82 ± 0.007 versus Flox: 1.0 ± 0.01, $P = 0.0004$; Figure 4A). Since misreading of Lys codon in proinsulin might cause aberrant processing, we investigated the C-peptide content, which indicates proper processing of proinsulin, in the pancreas of β cell KO and Flox mice. The C-peptide content in β cell KO pancreas was significantly lower than C-peptide content in Flox pancreas (β cell KO: 12.4 ± 1.41 ng/mg protein versus Flox: 22.4 ± 3.29 ng/ mg protein, $P = 0.0429$; Figure 4B). Accordingly, plasma C-peptide levels were significantly lower in β cell KO mice than in Flox mice (Figure 4C). Pancreatic sections were also immunostained with anti–C-peptide antibodies. Consistent with the reduction in C-peptide levels in β cell KO mice, the intensity of C-peptide stain-

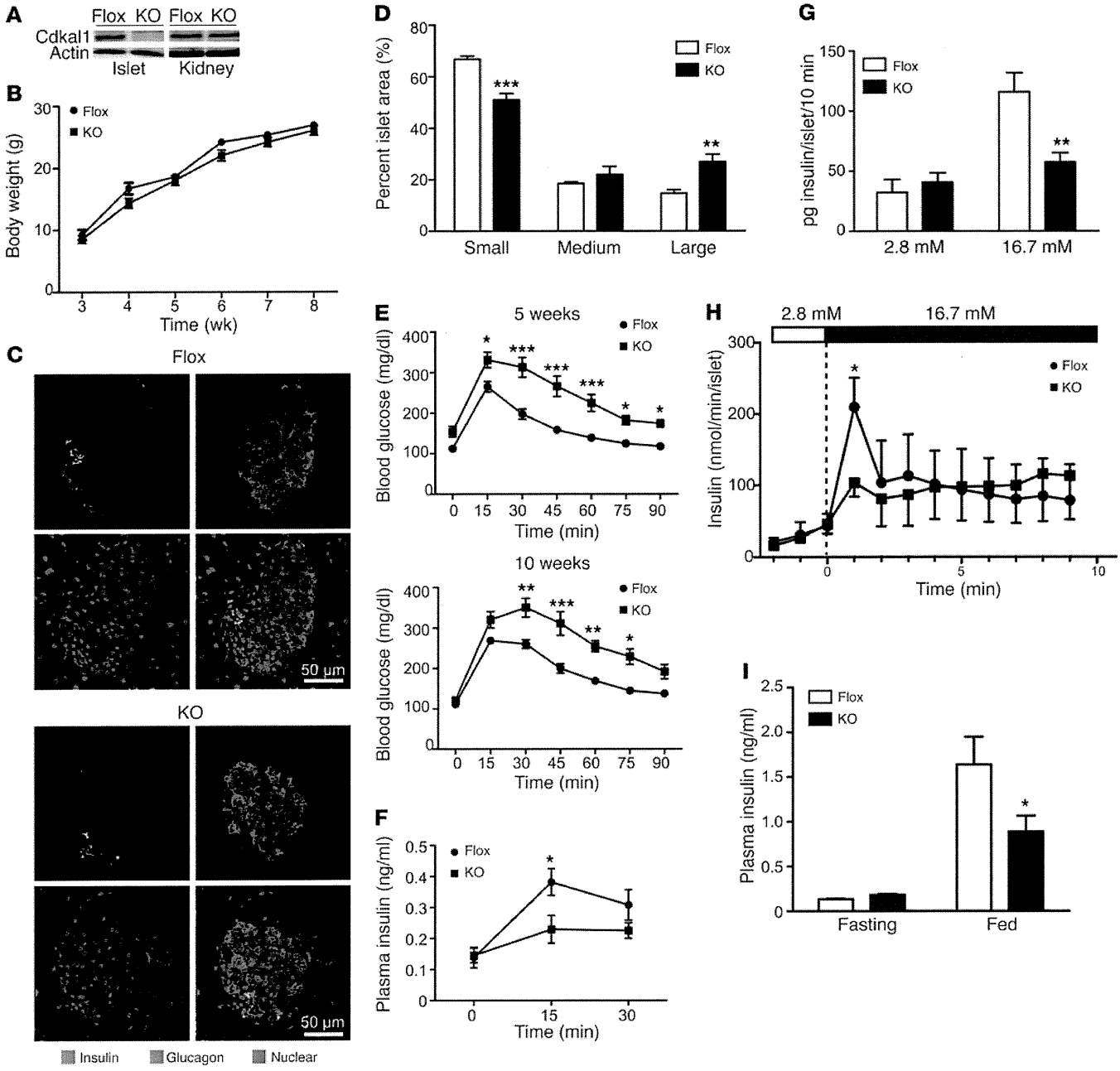

Figure 3

Conditional deletion of the *Cdkal1* gene causes glucose intolerance. (**A**) Conditional deletion of *Cdkal1* in pancreatic islets in β cell KO (KO) mouse. (**B**) Comparison of the body weights of β cell KO and Flox mice. (**C**) Pancreatic sections obtained from β cell KO and Flox mice at 5 weeks of age were immunostained with anti-insulin (red) and anti-glucagon (green) antibodies. Nuclei were counterstained with DAPI. (**D**) Comparison of relative islet area in pancreas of β cell KO and Flox mice. Area of 529 islets from 3 Flox mice and 572 islets from 3 β cell KO mice were examined and classified into small, medium, and large islet area. The relative distribution of each islet area was compared between β cell KO and Flox. (**E**) Blood glucose during glucose tolerance test at 5 weeks (upper) and 10 weeks (lower). $n = 4–7$. (**F**) Plasma insulin levels during a glucose tolerance test at 15 weeks. $n = 10–11$. (**G**) Glucose-stimulated insulin secretion in islets ($n = 8$) isolated from β cell KO or Flox mice was determined. (**H**) Glucose-stimulated insulin secretion in perfused islets of Flox and β cell KO mice. $n = 4–5$. (**I**) Plasma insulin levels in Flox or β cell KO mice fasted for 14 hours and re-fed for 1.5 hours. $n = 7$. Significant difference was examined by repeated measure of 2-way ANOVA (**E** and **F**) or 2-way ANOVA (**D**, **G**, and **I**) followed by Bonferroni's post-test or Mann-Whitney *U* test. Data are presented as mean ± SEM. $^*P < 0.05$; $^{**}P < 0.01$; $^{***}P < 0.001$ versus Flox.

ing was apparently reduced in KO islets compared with Flox islets (Supplemental Figure 9A). Previous study using pancreatic β cell-specific transgenic mice overexpressing mutant eIF2α has shown that aberrant protein translation could impair the correct targeting of proinsulin (22). Therefore, subcellular localization of proinsulin was investigated in β cell KO mice. High magnification revealed that proinsulin was mainly confined to the perinuclear area and colocalized with C-peptide in the β cells of Flox mice. In contrast,

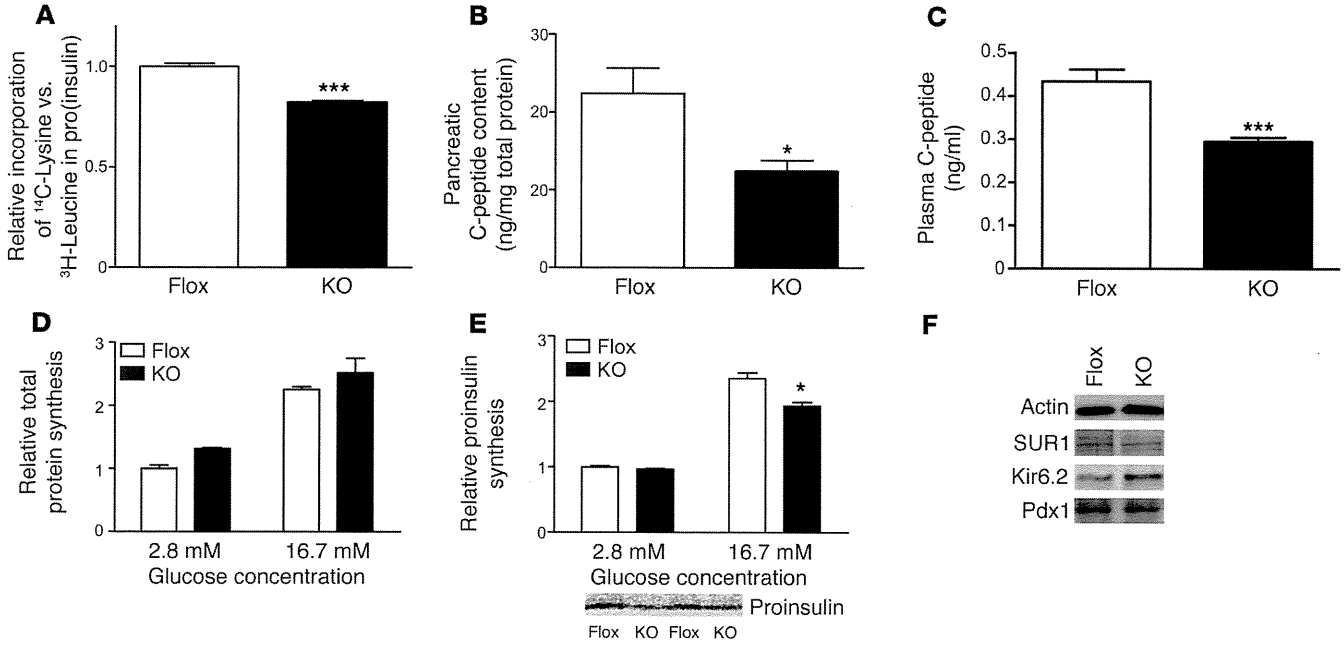

Figure 4

Aberrant insulin synthesis in the pancreatic β cells of β cell KO mice. (**A**) Relative incorporation of 14C-lysine to 3H-leucine in immunoprecipitated (pro)insulin in islets of β cell KO or Flox mice in KRB buffer containing 16.7 mM glucose for 1 hour. (**B**) Pancreatic C-peptide content of β cell KO or Flox mice was measured by ELISA, and value was normalized to total protein concentration. $n = 5–8$; $^{*}P < 0.05$ by Student's t test. (**C**) Plasma C-peptide concentrations in Flox and β cell KO mice fasted for 7 hours. $n = 10$. $^{***}P < 0.001$ by Student's t test. (**D**) Relative total protein synthesis under basal condition (2.8 mM) or stimulated condition (16.7 mM) was determined by normalizing 35S incorporation to the total protein concentration. $n = 4$; $^{*}P < 0.05$ by Student's t test. (**E**) Proinsulin synthesis in KO or Flox islets under basal condition (2.8 mM) or stimulated condition (16.7 mM) is shown in top panel. $n = 4$; $^{*}P < 0.05$ by Student's t test. (**F**) Expression of actin, SUR1, Kir6.2, and Pdx1 protein in islets of Flox or β cell KO mice determined by Western blotting. Results representative of 3 independent experiments are shown. All data are presented as mean ± SEM.

there were large aggregates of proinsulin-positive granules, which were not colocalized with C-peptide–positive granules in islets of β cell KO mice (Supplemental Figure 9B). These results suggest that Cdkal1 deficiency may cause abnormal proinsulin translation, which in turn leads to the impairment of both the processing and targeting of proinsulin.

In addition, we investigated the total protein synthesis level and proinsulin synthesis level in islets of β cell KO and Flox mice. Total protein synthesis in KO islets was not changed under either low- or high-glucose conditions (Figure 4D). There was no difference in proinsulin levels between KO islets and control islets under low-glucose conditions (Figure 4E). However, a significant decrease in proinsulin synthesis was observed in KO islets stimulated with high glucose compared with Flox islets (Figure 4E). A decrease in insulin synthesis was also observed in MIN6 cells transfected with siRNA targeting Cdkal1 (Supplemental Figure 10). To investigate whether Cdkal1 deficiency had any effect on the synthesis of other crucial β cell proteins, we examined the protein levels of Kir6.2, SUR1, and Pdx1. There were no obvious differences in protein levels between KO islets and Flox islets (Figure 4F). These results suggest that tRNA modification by Cdkal1 is crucial for translation fidelity and efficiency of proinsulin in pancreatic β cells.

Cdkal1 deficiency induces ER stress in β cells. Accumulation of unfolded or misfolded proteins in the ER lumen triggers stress response, which has been proposed to cause the dysfunction of pancreatic β cells (22–25). Notably, temporary or chronic imbalance in the protein synthesis environment can induce ER stress in β cells and subsequent glucose intolerance in vivo (22, 26, 27). To investigate whether aberrant proinsulin synthesis caused by Cdkal1 deficiency triggers stress responses in β cells, we examined the expression levels of a variety of genes essential for β cell function. There were no differences in the levels of insulin 1 or 2 mRNAs between KO and Flox islets (Figure 5A). Among pancreatic β cell marker genes, the mRNA levels of glucose transporter 2 (*Glut2*) were significantly reduced in KO islets (Figure 5B). Moreover, Glut2 was distributed diffusely in the cytoplasm of β cells in Cdkal1-deficient islets (Figure 5C). The decreased expression and abnormal localization of Glut2 correlate with ER stress (22). Therefore, the relative expression of ER stress–related genes was then examined in the pancreatic islets of β cell KO and Flox mice. Among all the stress-related genes, only the expression of spliced *Xbp1* was found to be elevated (Figure 5D). In addition, phospho-EIF2 levels were higher in KO islets than in Flox islets (Supplemental Figure 11). Furthermore, electron microscopy revealed distended ER, which indicates ER stress (27, 28), in pancreatic β cells from β cell KO mice but not from Flox mice (Figure 5E). These results suggest that *cdkal1* gene deficiency may induce an ER stress response and glucose intolerance.

Cdkal1 deficiency enhances susceptibility to high-fat diet stress. Environmental stress such as a high-fat diet (HFD) has a great impact on glucose metabolism. Interestingly, recent study has found the association of polymorphism in the *cdkal1* gene with the prevalence of metabolic syndrome in Japanese men (29). We therefore speculated that a HFD might induce profound glucose intolerance in β cell KO mice. To investigate the effect of an HFD, β cell KO and Flox mice

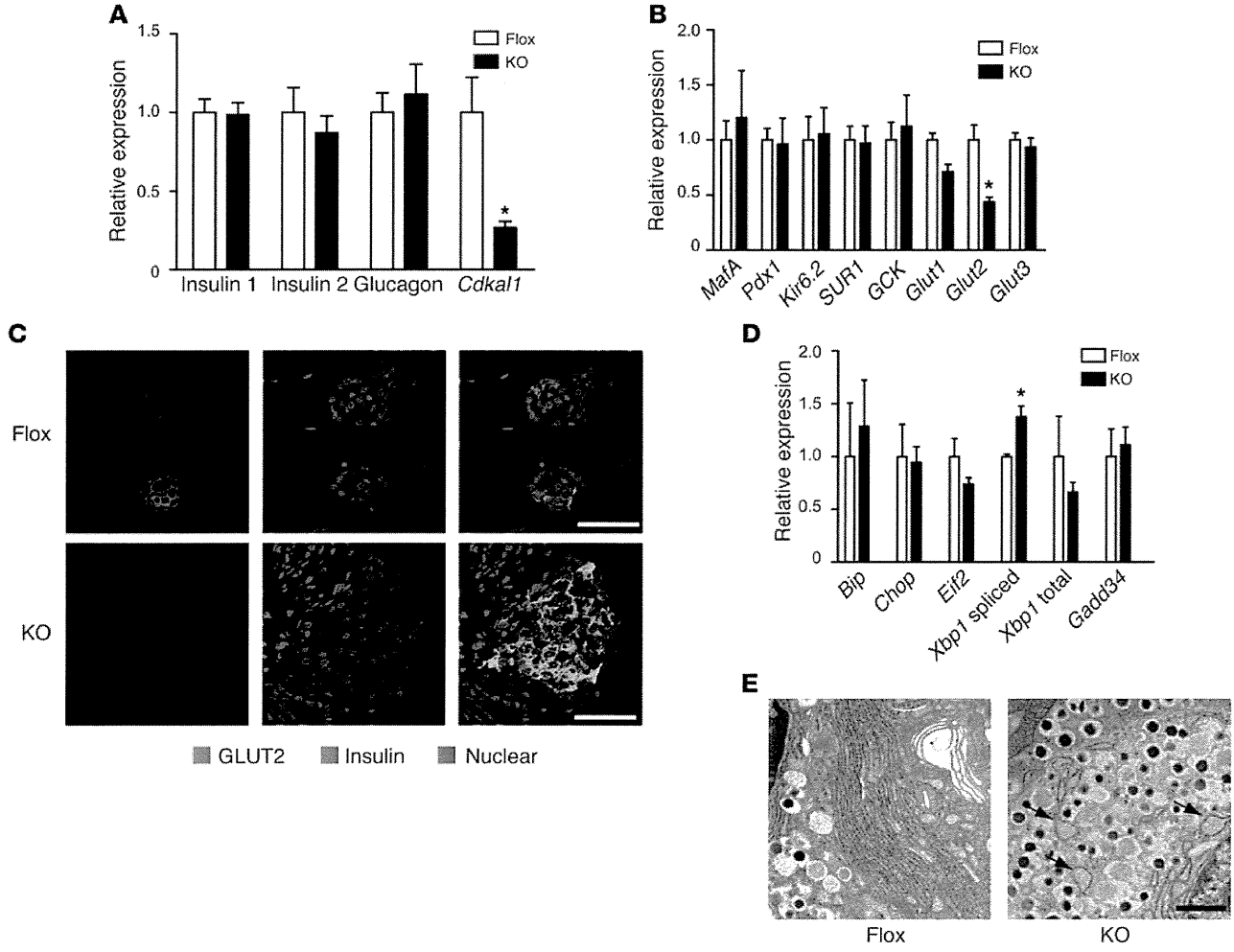

Figure 5

ER stress response in the pancreatic β cell KO mice. (**A**) Quantitative analysis of the mRNA expression of insulin, glucagon, and *Cdkal1* in isolated islets of β cell KO and Flox mice. $^*P < 0.05$; $n = 4$. (**B**) Comparison of the expression of β cell–related genes between β cell KO and Flox mice. $^*P < 0.05$; $n = 4$. (**C**) Subcellular distribution of GLUT2 in islets of β cell KO and Flox mice. Scale bars: 50 μm. (**D**) Quantitative analysis of ER stress–related genes in β cell KO and Flox mice. $^*P < 0.05$; $n = 4$. (**E**) Transmission electron microscopic examination of the ultrastructure of β cells in pancreatic sections of β cell KO mice and Flox mice. Arrows indicate the ER distention in the β cells of KO mice. Scale bar: 5 μm. Significant differences were examined by Student's *t* test (**A**, **B**, and **D**). All data are presented as mean ± SEM.

were fed either an HFD or a low-fat diet (LFD) for up to 8 weeks. There was no difference in weight gain between β cell KO and Flox mice during the experimental period (Figure 6A). Islet hypertrophy was observed in both β cell KO and Flox mice fed an HFD for 8 weeks as a compensatory effect of the diet (Supplemental Figure 12). However, significant glucose intolerance developed in β cell KO mice fed an HFD for 3 weeks, whereas Flox mice fed an HFD showed normal glucose tolerance compared with Flox mice fed an LFD (Figure 6B). Blood glucose levels at 15, 30, and 60 minutes after the intraperitoneal injection were higher in β cell KO mice than in Flox mice. After 8 weeks on an HFD, glucose intolerance was more severe in the β cell KO mice (Figure 6C). Blood glucose concentrations in β cell KO mice were continuously higher than control levels and increased 2 hours after a glucose injection (Figure 6C). In addition, both nonfasting blood glucose levels (Figure 6D) and 7 hour–fasting blood glucose levels (Figure 6E) were significantly higher in β cell KO mice than Flox mice after 3 weeks on an HFD, whereas nonfasting and 7 hour–fasting blood glucose levels in LFD-fed β cell KO mice were compatible with those in LFD-fed Flox mice (Figure 6, D and E). To investigate whether insulin sensitivity was affected in β cell KO mice, an insulin tolerance test was performed in β cell KO and Flox mice fed an HFD or LFD for 7 weeks. There were no differences in the action of insulin between β cell KO and Flox mice fed either diet (Figure 6F). We also investigated whether an HFD had any effect on liver function as well as counter-insulin responses such as glucagon production. To examine gluconeogenesis in the liver, Flox and β cell KO mice fed an HFD for 10 weeks were injected with pyruvate and blood glucose levels were measured. There was no significant difference in gluconeogenesis between Flox and β cell KO mice (Supplemental Figure 13A). Furthermore, we examined plasma glucagon levels in mice fed an HFD for 10 weeks. There was no difference in fasting glucagon levels between Flox and β cell KO mice (Supplemental Figure 13B). From these observations, we speculated that the severe glucose intolerance was mainly caused by HFD-induced ER stress and the consequent decrease in insulin secretion in Cdkal1

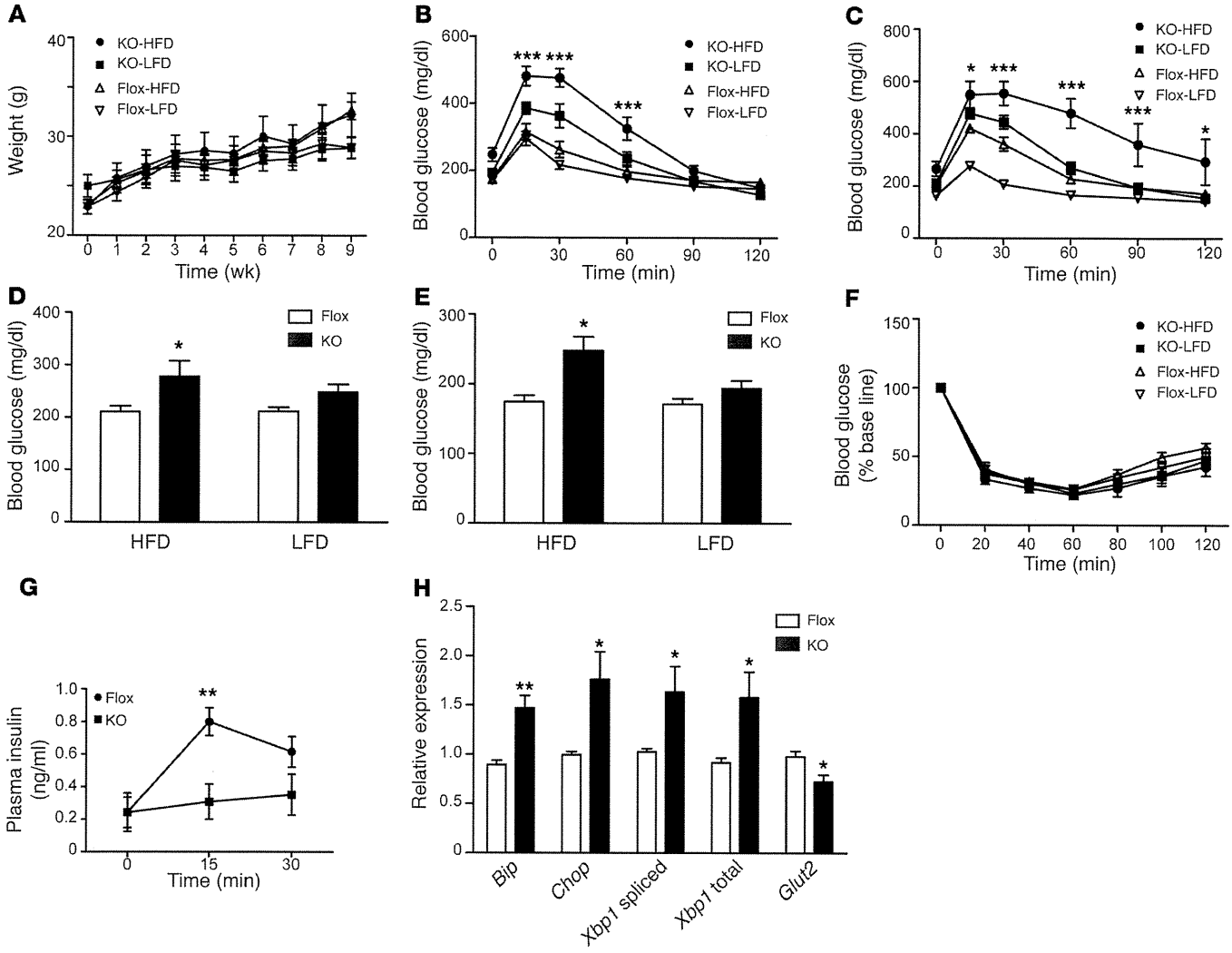

Figure 6

β cell KO mice exhibit increased ER stress and glucose intolerance after consuming an HFD. (**A**) Changes in body weight of β cell KO and Flox mice on an HFD and a LFD starting from 20 weeks old. (**B** and **C**) Results of the glucose tolerance test after 3 weeks (**B**) and 8 weeks (**C**) of consuming an HFD or a LFD. Mice were fasted for 7 hours from 8 am and injected with glucose (1 g/kg body weight). $^{*}P < 0.05$; $^{***}P < 0.001$, KO-HFD versus Flox-HFD mice. $n = 4–6$. (**D** and **E**) Nonfasting blood glucose (**D**) and 7-hour fasting blood glucose (**E**) levels after 3 weeks on an HFD or an LFD. $^{*}P < 0.05$; $n = 6$. (**F**) The insulin tolerance test was performed in mice fed an HFD or an LFD for 7 weeks. (**G**) β cell KO mice and Flox mice were fed an HFD for 8 weeks. Plasma insulin level during IPGTT (1 g/kg body weight) was examined in β cell KO mice and Flox mice fasted for 14 hours. $^{**}P < 0.01$; $n = 6$. (**H**) Relative expression of ER stress–related genes in β cell KO mice and Flox mice fed an HFD for 8 weeks. $^{**}P < 0.01$; $n = 4–5$. Significant differences between groups were examined by repeated measure of ANOVA (**A–C**, **F**, and **G**), 2-way ANOVA (**D** and **E**), or Student's *t* test (**H**). All data are presented as mean ± SEM.

KO β cells. Serum insulin levels after the injection of glucose were measured in β cell KO and Flox mice fed an HFD. Blood insulin levels after the challenge were significantly lower in β cell KO mice than in Flox mice (Figure 6G). Impaired glucose-stimulated insulin secretion was also observed in isolated Cdkal1-deficient pancreatic islets (Supplemental Figure 14). Finally, pancreatic islets were isolated from β cell KO mice and Flox mice fed the HFD for 8 weeks, and the expression levels of ER stress–related genes were examined (Figure 6H). We observed a significant increase in the expression of major ER stress–related genes, including the *Bip*, *CHOP*, and *Xbp1* genes. Our results indicate that Cdkal1 deficiency induces a massive ER stress response, which in turn decreases insulin secretion, causing severe glucose intolerance.

Discussion

Chemical modifications of nucleotides surrounding anticodons in tRNAs are believed to be essential for accuracy and efficiency in protein translation (14). The structural basis of the $ms^2i^6A^{37}$ modification at A^{37} of tRNA was recently identified in bacteria (30). The methylthiolation of i^6A^{37} is capable of stabilizing the codon-anticodon interaction through cross-strand stacking with the base of the first nucleotide of the mRNA codon. This stabilization of the codon-anticodon interaction prevents frame shifting and misreading during translation. In the present study, we showed that the ms^2t^6A modification of $tRNA^{Lys}(UUU)$ by Cdkal1 is required for the accurate translation of AAA and AAG codons. The human insulin gene contains 2 Lys(AAG) codons. One of the Lys residues

is located at the cleavage site between the C-peptide and A chain of insulin. Misreading of this Lys codon during insulin synthesis by ms^2t^6A modification–deficient $tRNA^{Lys}$(UUU) may cause the misfolding or miscleavage of proinsulin, which has an impact on glucose homeostasis. Indeed, we observed a decreased incorporation of lysine residue in Cdkal1-deficient β cells, as well as decreased C-peptide levels in pancreas of Cdkal1 KO. Interestingly, SNPs in the *Cdkal1* gene have been shown to associate with impaired conversion of proinsulin to insulin (31–33), supporting our finding that Cdkal1 deficiency may cause aberrant proinsulin generation.

The main role of pancreatic β cells is the adequate synthesis and release of insulin in response to glucose. To accomplish this task, the cells induce insulin biosynthesis in response to glucose. Proinsulin mRNA represents 20% of the total mRNA expression in glucose-stimulated β cells, whereas (pro)insulin biosynthesis approaches 50% of their total protein production (34, 35). It is inevitable that some insulin will be misfolded in such a mass production (36, 37). However, if augmented absolute levels of misfolded proinsulin are above the threshold, the misfolded proinsulin may lead to the inhibition of insulin production, ER stress, and β cell dysfunction. The onset of diabetes caused by misfolded proinsulin has been well studied in mutant INS gene–induced diabetes of youth (MIDY). In *Akita* mice, in which a heterozygous proinsulin-C(A7)Y mutation in the mouse *Ins2* gene is identical to the heterozygous mutation causing human MIDY, the mutant proinsulin in *Akita* mice blocks insulin production and activates ER stress in β cells (38, 39). On the other hand, dysregulation of protein synthesis can also lead to the production of misfolded proinsulin and ER stress. For example, a massive increase of protein synthesis by *Perk* deficiency causes massive proinsulin production, which leads to abnormal folding of proinsulin and ER stress (37). Taken together, these findings suggest that the absolute amount of misfolded proinsulin is a critical determinant of onset of ER stress followed by dysfunction of β cells. In β cell KO mice, the Cdkal1 deficiency may cause a certain amount of proinsulin to be mistranslated, which may be misfolded and accumulate in the ER, leading to further inhibition of insulin production and subsequent activation of ER stress.

A recent study showed impaired mitochondrial ATP generation, first-phase insulin exocytosis, and responsiveness of ATP-sensitive K^+ channel to glucose in general *Cdkal1*$^{-/-}$ mice (40). In β cell KO mice, we also observed impaired first-phase insulin secretion as well as impaired ATP generation after glucose stimulation (Figure 3H and Supplemental Figure 15). Considering the molecular function of Cdkal1, it is not assumed that Cdkal1 directly regulates these functions. These results suggest that aberrant protein translation may occur in the proteins involved in the regulation of mitochondrial ATP generation and insulin exocytosis in addition to insulin in Cdkal1-deficient mice. Although we did not detect obvious changes in the levels of Kir6.2 and SUR1, other proteins involved in mitochondrial functions may be abnormally translated and in turn cause the defect of ATP generation observed in KO islets.

In conclusion, our results suggest that functional loss of Cdkal1 affects the accuracy of protein translation, causing the synthesis of abnormal insulin, which triggers ER stress in β cells. These results provide evidence linking the molecular function of Cdkal1 with T2D.

Methods

Animals. Cdkal1$^{flox/flox}$ (Flox) mice were generated by flanking exon 5 of the *Cdkal1* gene with the loxP sequence (Supplemental Figure 8A). Flox mice were crossed with transgenic mice expressing Cre recombinase under the control of the rat insulin 2 promoter (RIP-Cre) to obtain pancreatic-specific Cdkal1 KO mice (Cdkal1$^{flox/flox;\ RIP\text{-}Cre/0}$: β cell KO). To delete Cdkal1 from all tissues, Flox mice were crossed with transgenic mice carrying Cre recombinase under the control of a CAG promoter (CAG-Cre) provided by RIKEN through a national bioresource project of the Ministry of Education, Culture, Sports, Science and Technology of Japan (MEXT). All mouse strains (Cdkal1$^{flox/flox}$, RIP-Cre, CAG-Cre) were backcrossed onto the C57BL/6 genetic background for more than 7 generations.

Animals were housed at 25°C with 12-hour light/12-hour dark cycles. High-fat chow (D12451, 45% kcal% fat) and low-fat chow (D12450B, 10% kcal% fat) were purchased from Research Diets. All animal procedures were approved by the Animal Ethics Committee of Kumamoto University (approval ID; A21-103).

Measurement of blood glucose and insulin levels. Mice were fasted for 14 hours (8:00 pm to 10:00 am) or 7 hours (8:00 am to 3:00 pm), followed by intraperitoneal injection of glucose (1 g/kg). Blood glucose was determined by a glucometer (ACCU-CHEK, Aviva; Roche). Plasma insulin or C-peptide levels were determined using an ELISA kit. To measure pancreatic C-peptide levels, whole pancreases were homogenized in an acid-ethanol solution. Pancreatic C-peptide levels were normalized to total protein concentration measured by BCA reagent (Pierce). For the insulin tolerance test, mice were injected with 1 unit/kg of regular human insulin. For pyruvate tolerance test, mice were fasted overnight and injected with sodium pyruvate (2 g/kg).

Morphological examination. For immunohistochemical examination, pancreatic sections were stained using anti-insulin (Santa Cruz Biotechnology Inc.), anti-glucagon (Sigma-Aldrich), and anti-GLUT2 (Santa Cruz Biotechnology Inc.) antibodies. Images were obtained using a FV1000 confocal microscope (Olympus). For islet morphological examination, pancreatic sections were examined as described previously (19). Pancreatic sections for transmission electron microscopic examination were prepared as described previously (41).

Gene expression studies. Islets were isolated from β cell KO mice or Flox mice by intraductal collagenase (Liberase TL grade; Roche) digestion followed by hand picking. Isolation of total RNA from islets was performed using an RNeasy Mini Kit (QIAGEN). A PrimerScript RT Reagent Kit was used to generate cDNA. Quantitative real-time PCRs were performed using either a TaqMan Gene Expression Kit (Applied Biosystems) or SYBR Premix Ex Taq. The results were normalized to the level of GAPDH or β actin. Primer sequences are provided in Supplemental Table 1.

Metabolic labeling experiments. Fifty islets were washed in Krebs-Ringer bicarbonate buffer (115 mM NaCl, 5 mM KCl, 10 mM $NaHCO_3$, 2.5 mM $MgCl_2$, 2.5 mM $CaCl_2$, and 20 mM HEPES, pH 7.4, 0.1% BSA) containing 2.8 mM glucose and incubated in the same buffer for 1 hour at 37°C. The buffer was then changed to incubation buffer (2.8 mM or 16.7 mM glucose) containing 100 μCi [^{35}S]-methionine and cysteine (Tran^{35}S-LABEL; MP Biomedical Inc.) for 1 hour. The islets were lysed in 100 μl of lysis buffer (50 mM HEPES, pH 7.4, 150 mM NaCl, 1% Triton X-100, 0.1% SDS, protease inhibitor cocktail; Roche). Then 5 μl of lysate was taken for a total protein assay using BCA reagent (Pierce), and 5 μl was taken for measurement of total protein synthesis by trichloroacetic acid precipitation on Whatman filter paper. Proinsulin synthesis was measured by immunoprecipitation of 50 μg of islet lysates with anti-insulin antibody (Santa Cruz Biotechnology Inc.) conjugated on protein A–Dynabeads (Invitrogen). Immunoprecipitated proteins were resolved on a Tris-Tricine gel (Invitrogen). The labeled proinsulin was quantified by FLP2000 (Fuji Film).

L-[^{14}C(U)]-lysine and L-[3,4,5-^{3}H(N)-leucine were purchased from PerkinElmer Life and Analytical Sciences. Fifty islets were washed in Krebs-Ringer bicarbonate buffer containing 2.8 mM glucose. The buffer was changed to incubation buffer (16.7 mM glucose) containing 10 μCi of L-[3,4,5-^{3}H(N)-leucine and 1 μCi L-[^{14}C(U)]-lysine for 1 hour. The islets were lysed

in 50 μl of lysis buffer (50 mM HEPES, pH 7.4, 150 mM NaCl, 0.5% Triton X-100, protease inhibitor cocktail; Roche). Lysates were precleared with Dynabeads Protein A for 1 hour to reduce background absorption to Dynabeads. Lysates were then incubated with guinea pig anti-insulin antibody (AB3440; Millipore) for 3 hours, and (pro)insulin was immunoprecipitated by adding Dynabeads Protein A. Immunoprecipitated proteins was eluted using nondenaturing elution buffer included in the Dynabeads immunoprecipitation kit (Invitrogen), and radioactivity was measured by a liquid scintillation counter (Aloka).

Analysis of ms^2t^6A modification in tRNA. Purification of total RNA from mouse tissues or a cultured cell line was performed using a guanidinium thiocyanate/phenol/chloroform method (42). Individual $tRNA^{Lys}$(UUU) or $tRNA^{Lys}$(CUU) was purified by reciprocal circulating chromatography (RCC) (43). Purified total RNA or individual tRNA was hydrolyzed to obtain nucleosides or digested to obtain oligonucleotides, then subjected to liquid chromatography/mass spectrometry (44).

Reporter assay for detecting frame-shifts in B. subtilis. Reporters for detecting translational fidelity were adapted from a luciferase-based reporter as described previously (16). For protein expression in *B. subtilis*, reporters were cloned into pHT01 vectors (MoBiTec). WT (trpC2) *B. subtilis* and *yqeV*-deficient (Δ*yqeV*) *B. subtilis* were obtained from the National BioResource Project (*B. subtilis*; NIG). Transformation of *B. subtilis* with a pHT01 vector containing each construct was performed according to the protocol of Anagnostopoulos and Spizizen (45). Colonies were cultured at 37°C in 2 ml LB medium containing 2.5 μg/ml chloramphenicol until OD_{600} = 0.5. Isopropyl β-D-1thiogalactopyranoside (IPTG) was added to cultures at a final concentration of 1 mM. After 1 hour of incubation, the cultures were harvested and lysed in lysis buffer (50 mM HEPES, pH 7.4, 100 mM KCl, 10 mM $MgCl_2$, 2 mg/ml lysozyme). Aliquots of 5 μl were used in the luciferase assay using the Dual-Luciferase Reporter Assay System (Promega).

Islet perifusion. Islets were isolated from Flox mice or β cell KO mice and cultured in RPMI medium with 10% FBS overnight. Seventy islets were loaded on a filter (Millipore) and perifused with KRB buffer with constant bubbling of 95% O_2 and 5% CO_2 for 30 minutes. Islets were then stimulated with KRB buffer containing 16.7 mM glucose. Islets were perifused with KRB buffer at a flow rate of 1 ml/min. Insulin levels were measured by ELISA as described above.

Biochemical assay. Western blotting was carried out as described elsewhere. The anti-Kir6.2 antibody was purchased from Sigma-Aldrich, anti-SUR1 antibody was from Santa Cruz Biotechnology Inc., and anti-Pdx1 antibody was from Millipore. ATP levels were measured in 25 islets using an ATP Bioluminescent Kit (Roche). Briefly, islets were incubated in KRB buffer containing 2.8 mM glucose for 30 minutes and then stimulated with KRB buffer containing either 2.8 mM glucose or 16.7 mM glucose for 30 minutes. The extraction and measurement of ATP in islets were performed according to protocols provided.

Statistics. All data are presented as mean ± SEM. Statistical significance of differences between groups was evaluated using 1-way ANOVA, 2-way ANOVA, repeated measure of 2-way ANOVA, 2-tailed Student's *t* test, and the Mann-Whitney *U* test. $P < 0.05$ was considered significant.

Acknowledgments

We thank E. Araki and T. Kondo for help with the immunohistochemistry, K. Asai for providing the materials and the technical advice for transformation of *B. subtilis*, and N. Maeda for technical assistance. This work was supported by a Grant-in-Aid for Scientific Research from the Ministry of Education, Culture, Sports, Science and Technology of Japan, by the Japan Society for the Promotion of Science (JSPS) through its Funding Program for Next Generation World-Leading Researchers, by the Uehara Memorial Foundation, and by the Takeda Science Foundation.

Received for publication March 17, 2011, and accepted in revised form June 8, 2011.

Address correspondence to: Kazuhito Tomizawa, Department of Molecular Physiology, Faculty of Life Sciences, Kumamoto University, 1-1-1 Honjyo, Kumamoto 860-8556, Japan. Phone: 81.96.373.5050; Fax: 81.96.373.5052; E-mail: tomikt@kumamoto-u.ac.jp.

1. Steinthorsdottir V, et al. Variant in CDKAL1 influences insulin response and risk of type 2 diabetes. *Nat Genet.* 2007;39(6):770–775.
2. Saxena R, et al. Genome-wide association analysis identifies loci for type 2 diabetes and triglyceride levels. *Science.* 2007;316(5829):1331–1336.
3. Scott LJ, et al. A genome-wide association study of type 2 diabetes in Finns detects multiple susceptibility variants. *Science.* 2007;316(5829):1341–1345.
4. Zeggini E, et al. Replication of genome-wide association signals in UK samples reveals risk loci for type 2 diabetes. *Science.* 2007;316(5829):1336–1341.
5. Dehwah MA, Wang M, Huang QY. CDKAL1 and type 2 diabetes: a globalmeta-analysis. *Genet Mol Res.* 2010;9(2):1109–1120.
6. Groenewoud MJ, et al. Variants of CDKAL1 and IGF2BP2 affect first-phase insulin secretion during hyperglycaemic clamps. *Diabetologia.* 2008;51(9):1659–1663.
7. Stancáková A, et al. Association of 18 confirmed susceptibility loci for type 2 diabetes with indices of insulin release, proinsulin conversion, and insulin sensitivity in 5,327 nondiabetic Finnish men. *Diabetes.* 2009;58(9):2129–2136.
8. Ruchat SM, et al. Association between insulin secretion, insulin sensitivity and type 2 diabetes susceptibility variants identified in genome-wide association studies. *Acta Diabetol.* 2009;46(3):217–226.
9. Arragain S, et al. Identification of eukaryotic and prokaryotic methylthiotransferase for biosynthesis of 2-methylthio-N6-threonylcarbamoyladenosine in tRNA. *J Biol Chem.* 2010; 285(37):28425–28433.
10. Pierrel F, Douki T, Fontecave M, Atta M. MiaB protein is a bifunctional radical-S-adenosylmethionine enzyme involved in thiolation and methylation of tRNA. *J Biol Chem.* 2004;279(46):47555–47563.
11. Hernandez HL, et al. MiaB, a bifunctional radical-S-adenosylmethionine enzyme involved in the thiolation and methylation of tRNA, contains two essential [4Fe-4S] clusters. *Biochemistry.* 2007; 46(17):5140–5147.
12. Urbonavicius J, Qian Q, Durand JM, Hagervall TG, Björk GR. Improvement of reading frame maintenance is a common function for several tRNA modifications. *EMBO J.* 2001;20(17):4863–4873.
13. Wilson RK, Roe BA. Presence of the hypermodified nucleotide N6-(delta2-isopentenyl)-2-methylthioadenosine prevents codon misreading by Escherichiacoli phenylalanyl-transfer RNA. *Proc Natl Acad Sci U S A.* 1989;86(2):409–413.
14. Agris PF. Decoding the genome: a modified view. *Nucleic Acids Res.* 2004;32(1):223–238.
15. Grosjean H, Sprinzl M, Steinberg S. Posttranscriptionally modified nucleosides in transfer RNA: their locations and frequencies. *Biochimie.* 1995;77(1–2):139–141.
16. Kimura S, Suzuki T. Fine-tuning of the ribosomal decoding center by conserved methyl-modifications in the Escherichia coli 16S rRNA. *Nucleic Acids Res.* 2010;38(4):1341–1352.
17. Kramer EB, Vallabhaneni H, Mayer LM, Farabaugh PJ. A comprehensive analysis of translational missense errors in the yeast Saccharomyces cerevisiae. *RNA.* 2010;16(9):1797–1808.
18. Kramer EB, Farabaugh PJ. The frequency of translational misreading errors in E. coli is largely determined by tRNA competition. *RNA.* 2007; 13(1):87–96.
19. Wei FY, et al. Cdk5-dependent regulation of glucose-stimulated insulin secretion. *Nat Med.* 2005; 11(10):1104–118.
20. Ching YP, Pang AS, Lam WH, Qi RZ, Wang JH. Identification of a neuronal Cdk5 activator-binding protein as Cdk5 inhibitor. *J Biol Chem.* 2002; 277(18):15237–15240.
21. Wang X, Ching YP, Lam WH, Qi Z, Zhang M, Wang JH. Identification of a common protein association region in the neuronal Cdk5 activator. *J Biol Chem.* 2000;275(41):31763–31769.
22. Back SH, et al. Translation attenuation through eIF2alpha phosphorylation prevents oxidative stress and maintains the differentiated state in beta cells. *Cell Metab.* 2009;10(1):13–26.
23. Eizirik DL, Cnop M. ER stress in pancreatic beta cells: the thin red line between adaptation and failure. *Sci Signal.* 2010;3(110):pe7.
24. Oslowski CM, Urano F. The binary switch between life and death of endoplasmic reticulum-stressed beta cells. *Curr Opin Endocrinol Diabetes Obes.* 2010; 17(2):107–112.
25. Scheuner D, Kaufman RJ. The unfolded protein response: a pathway that links insulin demand

with beta-cell failure and diabetes. *Endocr Rev.* 2008; 29(3):317–333.
26. Han D, et al. IRE1alpha kinase activation modes control alternate endoribonuclease outputs to determine divergent cell fates. *Cell.* 2009; 138(3):562–575.
27. Scheuner D, et al. Control of mRNA translation preserves endoplasmic reticulum function in beta cells and maintains glucose homeostasis. *Nat Med.* 2005;11(7):757–764.
28. Sachdeva MM, et al. Pdx1 (MODY4) regulates pancreatic beta cell susceptibility to ER stress. *Proc Natl Acad Sci U S A.* 2009;106(45):19090–19095.
29. Miyaki K, et al. Association of a cyclin-dependent kinase 5 regulatory subunit-associated protein 1-like 1 (CDKAL1) polymorphism with elevated hemoglobin A_1(c) levels and the prevalence of metabolic syndrome in Japanese men: interaction with dietary energy intake. *Am J Epidemiol.* 2010; 172(9):985–991.
30. Jenner LB, Demeshkina N, Yusupova G, Yusupov M. Structural aspects of messenger RNA reading frame maintenance by the ribosome. *Nat Struct Mol Biol.* 2010;17(5):555–560.
31. Kirchhoff K, et al. Polymorphisms in the TCF7L2, CDKAL1 and SLC30A8 genes are associated with impaired proinsulin conversion. *Diabetologia.* 2008; 51(4):597–601.
32. Stancáková A, et al. Association of 18 confirmed susceptibility loci for type 2 diabetes with indices of insulin release, proinsulin conversion, and insulin sensitivity in 5,327 nondiabetic Finnish men. *Diabetes.* 2009;58(9):2129–213.
33. Haupt A, et al. The risk allele load accelerates the age-dependent decline in beta cell function. *Diabetologia.* 2009;52(3):457–462.
34. Van Lommel L, et al. Probe-independent and direct quantification of insulin mRNA and growth hormone mRNA in enriched cell preparations. *Diabetes.* 2006;55(12):3214–3220.
35. Schuit FC, In't Veld PA, Pipeleers DG. Glucose stimulates proinsulin biosynthesis by a dose-dependent recruitment of pancreatic beta cells. *Proc Natl Acad Sci U S A.* 1988;85(11):3865–3869.
36. Schubert U, Antón LC, Gibbs J, Norbury CC, Yewdell JW, Bennink JR. Rapid degradation of a large fraction of newly synthesized proteins by proteasomes. *Nature.* 2000;404(6779):770–774.
37. Liu M, Li Y, Cavener D, Arvan P. Proinsulin disulfide maturation and misfolding in the endoplasmic reticulum. *J Biol Chem.* 2005;280(14):13209–13212.
38. Wang J, et al. A mutation in the insulin 2 gene induces diabetes with severe pancreatic beta-cell dysfunction in the Mody mouse. *J Clin Invest.* 1999; 103(1):27–37.
39. Yoshioka M, Kayo T, Ikeda T, Koizumi A. A novel locus, Mody4, distal to D7Mit189 on chromosome 7 determines early-onset NIDDM in nonobese C57BL/6 (Akita) mutant mice. *Diabetes.* 1997; 46(5):887–894.
40. Ohara-Imaizumi M, et al. Deletion of CDKAL1 affects mitochondrial ATP generation and first-phase insulin exocytosis. *PLoS One.* 2010; 5(12):e15553.
41. Han XJ, et al. CaM kinase I alpha-induced phosphorylation of Drp1 regulates mitochondrial morphology. *J Cell Biol.* 2008;182(3):573–585.
42. Chomczynski P, Sacchi N. The single-step method of RNA isolation by acid guanidinium thiocyanate-phenol-chloroform extraction: twenty-something years on. *Nat Protoc.* 2006;1(2):581–585.
43. Miyauchi K, Ohara T, Suzuki T. Automated parallel isolation of multiple species of non-coding RNAs by the reciprocal circulating chromatography method. *Nucleic Acids Res.* 2007;35(4):e24.
44. Ikeuchi Y, et al. Agmatine-conjugated cytidine in a tRNA anticodon is essential for AUA decoding in archaea. *Nat Chem Biol.* 2010;6(4):277–282.
45. Anagnostopoulos C, Spizizen J. Requirement for Transformation in Bacillus subtilis. *J Bacteriol.* 1961;81(5):741–746.

Endocrine Journal 2011, **58** (10), 819-825

REVIEW

Functional loss of Cdkal1, a novel tRNA modification enzyme, causes the development of type 2 diabetes

Fan-Yan Wei and Kazuhito Tomizawa

Department of Molecular Physiology, Faculty of Life Sciences, Kumamoto University, Kumamoto 860-8556, Japan

Abstract. A number of whole-genome association studies show the *cdk5 regulatory associated protein 1-like 1* (*cdkal1*) gene to be one of the most reproducible risk genes in type 2 diabetes (T2D). Variations in the gene are associated with impaired insulin secretion but not insulin resistance or obesity. Although the physiological functions of Cdkal1 had been unclear, recent studies show that it is a tRNA modification enzyme, a mammalian methylthiotransferase that biosynthesizes 2-methylthio-N^6-threonylcarbamoyladenosine (ms^2t^6A) at position 37 of $tRNA^{Lys}(UUU)$. The ms^2t^6A modification in $tRNA^{Lys}(UUU)$ is important for preventing the misreading of its cognate codons, especially when the rate of translation is relatively high. In both general and pancreatic β-cell-specific *cdkal1*-deficient mice, impaired mitochondrial ATP generation and first-phase insulin secretion are observed. Moreover, the β-cell-specific knockout mice show pancreatic islet hypertrophy and impaired blood glucose control. The mice are also hypersensitive to high-fat diet-induced endoplasmic reticulum (ER) stress. In this review, we provide an overview of the physiological functions of Cdkal1 and the molecular pathogenesis of T2D in patients carrying *cdkal1* risk alleles.

Key words: Insulin synthesis, Translation, Endoplasmic reticulum (ER), Cdk5, SNPs

TYPE 2 DIABETES (T2D), which is caused by a combination of environmental and genetic factors, affects > 200 million individuals worldwide, and its prevalence continues to increase in many countries [1]. T2D is characterized by an insulin secretory dysfunction of pancreatic β-cells combined with insulin resistance [2], but the primary mechanisms are still debated [3]. Important advances in the genetics of T2D have come with the completion of genome-wide association studies (GWASs) based on common HapMap single nucleotide polymorphisms (SNPs) and the properties and power of analytical tests to detect such associations [4]. GWASs have currently led to the discovery of 38 risk genes in which there are variations associated with T2D [5]. One of the genes with the most reproducible risk across different ethnic populations is *cdkal1* [1, 6-8]. Here, we present the physiological functions of Cdkal1 and the phenotype of β-cell-knockout mice.

Submitted Jun. 28, 2011; Accepted Jul. 5, 2011 as EJ11-0099
Released online in J-STAGE as advance publication Sep. 8, 2011

Correspondence to: Kazuhito Tomizawa, Department of Molecular Physiology, Faculty of Life Sciences, Kumamoto University, 1-1-1 Honjyo, Kumamoto 860-8556, Japan.
E-mail: tomikt@kumamoto-u.ac.jp

1. Association of variants in *cdkal1* with T2D

There are five SNPs associated with T2D in the *cdkal1* gene (Fig. 1) [9]. All of the SNPs are located in intron 5 of *cdkal1* on 6p22.3, suggesting that they are noncoding SNPs (Fig. 1A). Although what biological role these noncoding SNPs may play is still unclear, it is speculated that they are involved in the regulation of Cdkal1 expression and the formation of splicing variants. The strongest associations with T2D are observed for rs7754840 and rs10946398, which are in complete linkage disequilibrium (r2 = 1.0 according to HapMap-CEU) [6, 10]. Moreover, an association of the G allele of rs 7756992 with T2D was reported in an Icelandic study, and this association was replicated in the combined data from five case-control studies of European ancestry and Asian populations [7].

GWASs show the association of SNPs in *cdkal1* with some pathological characteristics of T2D. Homozygous carriers of the risk allele of rs7756992 have an estimated 22% lower corrected insulin response (CIR) to an oral glucose load than non-carriers ($P = 3.5 \times 10^{-9}$) [7]. The risk allele of rs7754840 is also associated with reduced insulin secretion, measured as an insulinogenic

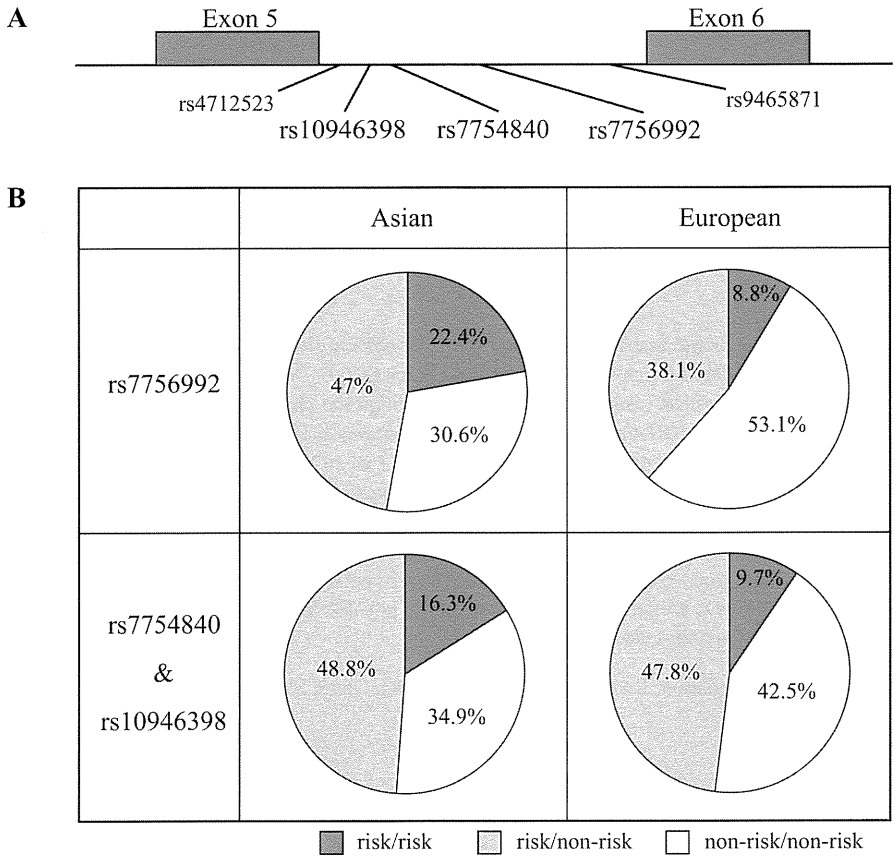

Fig. 1 Variants in the *cdkal1* gene associated with T2D. **A**. The location of SNPs associated with T2D in *cdkal1* gene. **B**. Comparison of the ratio of the risk and non-risk alleles in *cdkal1* between Asian and European populations.

index (IGI), in subjects without T2D (P = 0.01) [6]. Among nondiabetic offspring of T2D subjects, carriers of the GC and CC genotypes of rs775480 had 11 and 24% lower first-phase insulin release in an intravenous glucose tolerance test (IVGTT) than did carriers of the GG genotype (P = 0.002) [9]. The C allele was also associated with a higher glucose area under the curve in an oral glucose tolerance test (OGTT) (P = 0.016) [9]. In 533 patients with T2D and 3367 nondiabetic subjects, rs775480 was associated with impaired insulin release (IGI, P = 0.012) [9]. Moreover, a recent study showed that the CC genotype of rs9465871 was associated with elevated glycosylated hemoglobin A_{1c} (HbA1c) levels [11]. These results suggest that variants in *cdkal1* influence the risk of T2D from impaired insulin secretion and the Cdkal1 protein may be involved in the regulation of insulin secretion. In contrast, the gene variants are not associated with insulin sensitivity or obesity [9, 12]. The association of the variants of *cdkal1* with T2D is observed across different ethnic populations [7, 8, 11, 13]. Interestingly, the ratio of the risk allele of *cdkal1* is higher in Asian than European populations (Fig. 1B). Takeuchi *et al* [13] reported that *cdkal1* was the best-replicated susceptibility locus and the strongest associated with T2D among several susceptibility loci, including *KCNQ1*, in the Japanese population. Asian-type T2D is characterized by a larger decrease in insulin secretion and less insulin resistance or obesity [14, 15]. Thus, the variants of *cdkal1* may be implicated in T2D in Asian populations.

2. Physiological functions of Cdkal1

Although a number of GWASs (> 90 papers) show an association of the SNPs in *cdkal1* with T2D, physiological functions had been cloaked in mystery. As the full name shows, the amino acid sequence is highly similar with Cdk5 regulatory-associated protein 1 (Cdk5rap1), which was discovered as a binding protein of the Cdk5 regulatory subunit, p35 and p39 [16]. Cdk5rap1 inhib-

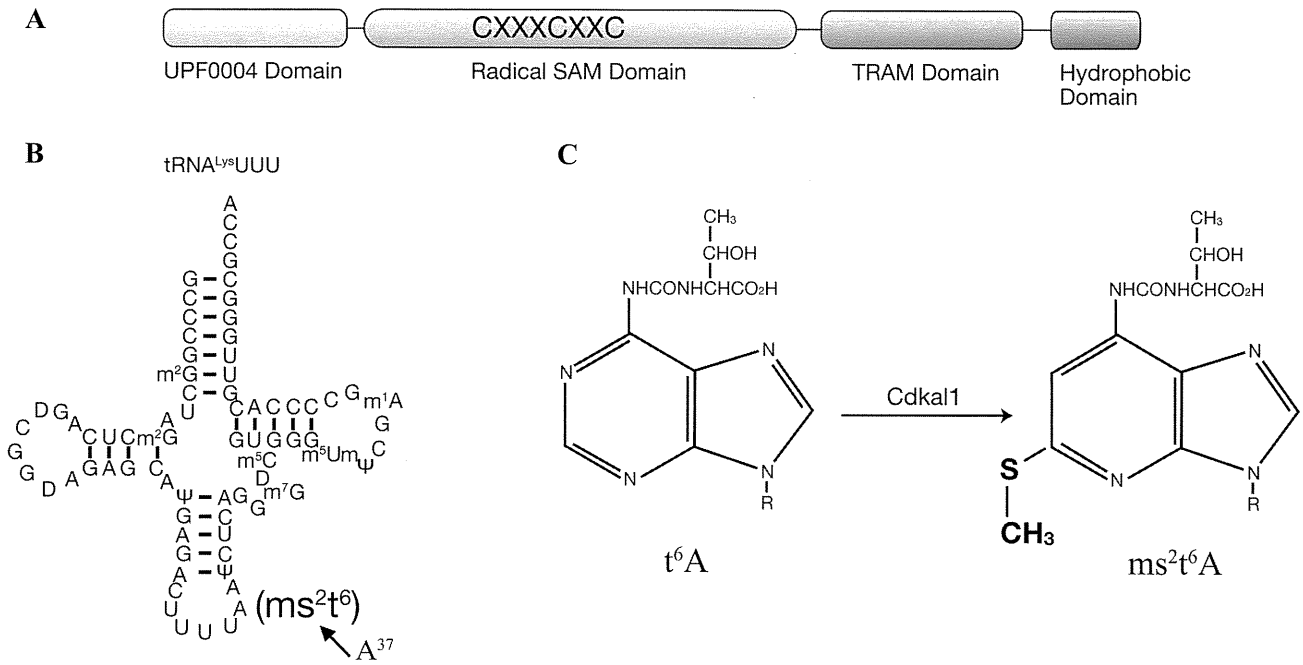

Fig. 2 Cdkal1 structure and modification of $tRNA^{Lys}$(UUU) by Cdkal1. **A**. Primary structure of Cdkal1. **B**. $tRNA^{Lys}$(UUU) modification by Cdkal1. Cdkal1 catalyzes the change to adenosine at position 37 (A^{37}), 3'-adjacent to the anticodon. **C**. Methylthiolation of t^6A by Cdkal. Cdkal1 catalyzes the methylthiolation of t^6A to synthesieze ms^2t^6A.

its Cdk5 activity through interaction with p35 and p39 [16]. As Cdk5 regulates insulin secretion [17, 18], it is postulated that Cdkal1 may regulate insulin secretion through the regulation of Cdk5 activity. However, Cdkal1 has no ability to interact with Cdk5 activators and no effect on Cdk5 activity [19, 20].

The primary structure of Cdkal1 has features of the methylthiotransferase (MTTase) family, a subclass of the large radical AdoMet enzyme superfamily [21]. The MTTase family catalyzes chemically challenging reactions, in all cases involving a C-H to C-SCH_3 bound conversion, through a radical mechanism [21]. These reactions participate in important biological processes such as tRNA or ribosomal protein modification [22-25]. Cdkal1 contains the conserved domains [UPF0004, radical *S*-adenosyl-$_L$-methionine (SAM) and TRAM domains] of the MTTase family (Fig. 2A). The enzymes contain two [4Fe-4S] clusters [24, 25]. The first cluster is chelated by the three cysteines of a conserved *CXXXCXXC* motif in the radical SAM domain [26]. This cluster serves to bind and reduce AdoMet into methionine and the highly reactive 5'-deoxyadenosyl radical [27]. The second cluster is supposed to abstract an H atom of the substrate (tRNA or protein) selectively, thus generating an intermediate substrate radical that is amenable to C-S bond formation [27]. The thiolation step involves the second [4Fe-4S] cluster, chelated by three other conserved cysteines in the N-terminal UPF0004 domain [24, 25]. The final methylation step involves a second molecule of AdoMet [24, 25]. The C-terminal TRAM domain is involved in substrate (tRNA or protein) recognition, resulting in a specific signature of the MTTase family not shared by the other radical AdoMet proteins [25, 28]. Interestingly, the C-terminal hydrophobic domain exists only in Cdkal1 (Fig. 2A) and the domain contributes to the localization on the endoplasmic reticulum (ER) [20].

In amino acid sequence, Cdkal1 is highly similar to MiaB and YqeV, which are bacterial MTTase proteins [21]. Both MiaB and YqeV are involved in the methylthiolational modifications of tRNA from bacteria to mammals. MiaB catalyzes the methylthiolation of N^6-isopentenyladenosine (i^6A) to generate 2-methylthio-N^6- isopentenyladenosine (ms^2i^6A) at position 37 (A^{37}), 3'-adjacent to the anticodon in some tRNAs [22, 29]. In contrast, YqeV catalyzes the methylthiolation of N^6-threonyl carbamoyladenosine (t^6A) to synthesize 2-methylthio-N^6-threonyl carbamoyladenosine (ms^2t^6A) for tRNA in bacteria [21]. Cdkal1 is a mammalian methylthiotransferase that biosynthe-

sizes $ms^2t^6A^{37}$ in tRNA (Fig. 2B) [20]. Furthermore, Cdkal1 catalyzes the methylthiolation of t^6A to synthesize ms^2t^6A only for $tRNA^{Lys}$(UUU) in mammals (Fig. 2C) [20]. Thus, Cdkal1 is identified as a tRNA modification enzyme for $tRNA^{Lys}$(UUU).

3. Regulation of translational fidelity by Cdkal1-dependent tRNA modification

Chemical modification of A^{37} of tRNA has critical roles in regulating translational fidelity. For instance, the 2-methylthio modification (ms^2i^6A) is important for preventing the misreading and frame-shifting of cognate codons during protein translation in bacteria [30]. The structural basis of the $ms^2i^6A^{37}$ modification at A^{37} of tRNA was recently identified in bacteria [30, 31]. The methylthiolation (ms^2) of i^6A^{37} is capable of stabilizing the codon-anticodon interaction through cross-strand stacking with the base of the first nucleotide of the mRNA codon [32]. This stabilization of the codon-anticodon interaction thus prevents frame shifting and misreading during translation.

Because the chemical structure of ms^2t^6A is highly similar to that of ms^2i^6A, it is conceivable that the ms^2t^6A modification is also required for translational accuracy when decoding Lys codons (AAA and AAG). Supporting this hypothesis, a previous *in vitro* study revealed that the ms^2t^6A modification in A^{37} of $tRNA^{Lys}$(UUU) increased the strength of the codon-anticodon interaction [33]. To examine whether the ms^2t^6A modification prevents either the frame-shifting or misreading of $tRNA^{Lys}$(UUU)'s cognate codons (AAA and AAG) *in vivo*, we utilized a dual luciferase-based reporter assay in WT *Bacillus subtilis* and *yqeV*-deficient *Bacillus subtilis* (Δ*yqeV*), which lacks the ms^2t^6A modification in A^{37} of $tRNA^{Lys}$(UUU) [20]. Luciferase-based reporter assays are particularly suitable for examining the function of the ms^2t^6A modification, because Lys529 in *firefly* luciferase is essential for enzymatic activity, and any misreading of Lys529 thus causes a reduction in lucifearse activity. We observed a significant decrease of *firefly* luciferase activity in Δ*yqeV* compared to the wild-type strain, reflecting misreading of the Lys codon due to the deficiency of the ms^2t^6A modification in the Δ*yqeV* strain [20]. Taken together, these results suggest the ms^2t^6A modification to be important for accurate decoding of the Lys codon by stabilizing codon-anticodon interactions.

4. Glucose intolerance in pancreatic β cell-specific Cdkal1-knockout mice

Individuals carrying risk variants in *cdkal1* show decreased first-phase insulin secretion with normal peripheral insulin sensitivity [9, 12]. These results suggest that pancreatic β-cells may be susceptible to the risk variants in the *cdkal1* gene. To investigate the physiological functions of Cdkal1 in pancreatic β-cells, β-cell-specific Cdkal1-deficient mice (KO mice) were generated [20]. KO mice showed normal development compared with their littermate controls (Flox) [20]. However, KO mice exhibited glucose intolerance, whereas the peripheral insulin sensitivity was normal. Plasma insulin levels after glucose treatment were lower in KO mice than Flox mice. Notably, first-phase insulin secretion was significantly lower in perfused KO islets than Flox islets [20]. We also observed a defect of glucose-induced ATP generation in KO islets [20]. It is worth stressing that the impairment of both first-phase insulin secretion and ATP generation was also observed in general Cdkal1-deficient mice [19].

Furthermore, β-cell-specific Cdkal1-deficient mice (KO mice) were hypersensitive to a high-fat diet. Only three weeks of high-fat-diet feeding, which did not induce apparent glucose intolerance in Flox mice, significantly induced severe glucose intolerance as well as impairments of insulin secretion in KO mice [20]. These findings clearly show that Cdkal1 deficiency could impair first-phase insulin secretion, which leads to glucose intolerance. Furthermore, the phenotypes observed in KO mice are very similar to those in T2D patients carrying risk variants in *Cdkal1*, suggesting that Cdkal1 deficiency may explain the molecular pathogenesis of T2D in these patients (Fig. 3).

5. Mistranslation of proinsulin and increase in ER stress response by Cdkal1 deficiency

The stress response evoked by the accumulation of unfolded proteins in ER has been implicated in the development of T2D [34]. Evidence of the ER stress response in diabetes has emerged from studies of Mutant INS-gene-induced diabetes of youth (MIDY). Mutations in the *proinsulin* gene directly cause misfolding of proinsulin, which leads to a severe ER stress response and subsequent β-cell dysfunction [35, 36]. Moreover, proteins related to the ER stress response, such as Bip, CHOP, and $p58^{IPK}$, are upregulated in

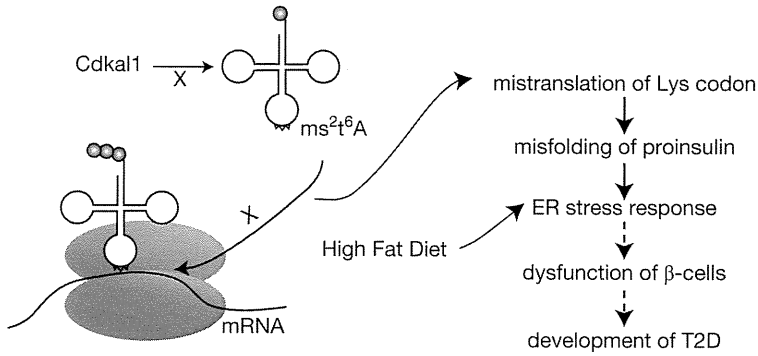

Fig. 3 Proposed working model for regulation of β-cell function by Cdkal1. Cdkal1 regulates translational fidelity by catalyzing the ms^2t^6A modification at A^{37} of $tRNA^{Lys}(UUU)$. A deficiency of the ms^2t^6A modification caused by the knockout of *cdkal1* or possibly risk variants in *cdkal1* would result in mistranslation of the Lys codon, and thus cause misfolding of proinsulin and a subsequent ER stress response. The ER stress response would decrease insulin secretion and ultimately cause dysfunction of β-cells. Environmental stress, such as a high-fat diet, would exaggerate the demand for insulin production, which enhances the ER stress response and dysfunction of β-cells, leading to the development of T2D.

β-cells from T2D patients compared with nondiabetic patients [37]. These findings strongly suggest that the ER stress response contributes to the development of diabetes. However, unlike the case for MIDY, there is no direct evidence of the presence of unfolded proteins in β-cells from T2D patients.

Given the molecular function of Cdkal1 in *Bacillus subtilis* as described above, it is conceivable that a deficiency in the proper modification of tRNA could trigger mistranslation, resulting in the accumulation of misfolded or unfolded proteins. In pancreatic β-cells of Cdkal1 KO mice, a deficiency of the ms^2t^6A modification in $tRNA^{Lys}(UUU)$ decreased the incorporation of Lysine into proinsulin, indicative of the mistranslation of proinsulin [20]. The Lys residue is particularly important for processing proinsulin to generate mature insulin and C-peptide, because one of the two Lys residues in human proinsulin is located at the cleavage site between the C-peptide and A chain of insulin. Mistranslation of the Lys codon in proinsulin may inhibit cleavage and subsequent generation of C-peptide. Indeed, the C-peptide level in the KO mice was significantly decreased compared to that in Flox mice [20]. As a consequence of the mistranslation of proinsulin, ER structures were abnormally dilated and spliced Xbp1, a gene product related to the ER stress response, was increased in β-cells of KO mice [20]. Furthermore, there was a global upregulation of genes related to the ER stress response, such as Bip and CHOP, in pancreatic β-cells of KO mice fed a high-fat diet for 8 weeks [20]. Taken together, these findings suggest a deficiency of the ms^2t^6A modification in $tRNA^{Lys}(UUU)$ to cause the mistranslation of proinsulin, which in turn leads to the accumulation of misfolded proinsulin and subsequent ER stress response (Fig. 3). Interestingly, risk variants in the *cdkal1* gene have been shown to associate with the impaired conversion of proinsulin to insulin [38, 39]. Thus, Cdkal1 deficiency may cause aberrant proinsulin generation and a consequent decrease in insulin secretion (Fig. 3).

6. Conclusion and perspective

Variants in the *cdkal1* gene have been reproducibly associated with decreased first-phase insulin secretion and the development of T2D [6-9, 11, 12]. Cdkal1 is a unique enzyme that catalyzes the ms^2t^6A modification in $tRNA^{Lys}(UUU)$ in mammalian cells [20]. Functional loss of Cdkal1 affects the accuracy of protein translation, causing the synthesis of abnormal insulin, which triggers ER stress in β-cells [20]. These findings provide evidence linking the molecular function of Cdkal1 with T2D. Nevertheless, to fully understand the molecular mechanism underlying risk variant-associated T2D, it is necessary to address whether risk variants in *cdkal1* could ultimately impact the enzymatic activity of Cdkal1 in T2D patients.

Acknowledgements

This work was supported by the Japan Society for the Promotion of Science (JSPS) through its "Funding Program for Next Generation World-Leading Researchers", by the Uehara Memorial Foundation, by the Takeda Science Foundation and by Yamada Bee Farm Grant for Honeybee Research.